

A mathematical model of the COVID-19 pandemic dynamics with dependent variable infection rate

Application to the Republic of Korea

Aycil Cesmelioglu · Kenneth L. Kuttler ·
Meir Shillor · Anna M. Spagnuolo

Received: date / Accepted: date

Abstract This work constructs, analyzes, and simulates a new compartmental SEIR-type model for the dynamics and potential control of the current COVID-19 pandemic. The novelty in this work is two-fold. First, the population is divided according to its compliance with disease control directives (lockdown, shelter-in-place, masks/face coverings, physical distancing, etc.) into those who fully comply and those who follow the directives partially, or are necessarily mobile (such as medical staff). This split, indirectly, reflects on the quality and consistency of these measures. This allows the assessment of the overall effectiveness of the control measures and the impact of their relaxing or tightening on the disease spread. Second, the adequate contact rate, which directly affects the infection rate, is one of the model unknowns, as it keeps track of the changes in the population behavior and the effectiveness of various disease treatment modalities via a differential inclusion. Existence, uniqueness and positivity results are proved using a nonstandard convex analysis based approach. As a case study, the pandemic outbreak in the Republic of Korea (South Korea) is simulated. The model parameters were found by minimizing the deviation of the model prediction from the reported data over the first 100 days of the pandemic in South Korea. The simulations show that the model captures accurately the pandemic dynamics in the subsequent 75

Aycil Cesmelioglu

Department of Mathematics and Statistics, Oakland University, Rochester, MI, USA E-mail: cesmelio@oakland.edu *ORCID ID: 0000-0001-8057-6349*

Kenneth L. Kuttler

retired, USA E-mail: klkuttler@gmail.com

Meir Shillor

Department of Mathematics and Statistics, Oakland University, Rochester, MI, USA E-mail: shillor@oakland.edu *ORCID ID: 0000-0001-6811-9524*

Anna M. Spagnuolo

Department of Mathematics and Statistics, Oakland University, Rochester, MI, USA E-mail: spagnuolo@oakland.edu *ORCID ID: 0000-0003-3039-0970*

days, which provides confidence in the model predictions and its future use. In particular, the model predicts that about 40% of the infections were not documented, which implies that asymptomatic infections contribute silently but substantially to the spread of the disease indicating that more widespread asymptomatic testing is necessary.

Keywords COVID-19 · SARS-CoV-2 · compartmental continuous model · nonlinear fitting · simulations

Mathematics Subject Classification (2010) MSC 92D30 · 92B05 · 92B99 · 34A60 · 34F05

1 Introduction

The novel coronavirus SARS-CoV-2 emerged in Wuhan, China, in December 2019 as a mutation of the Severe Acute Respiratory Syndrome Coronavirus, SARS-CoV. The first group of COVID-19 patients, reported in Wuhan exhibited flu-like symptoms resulting in the serious cases in pneumonia and death. There is mounting evidence (Huang et al. 2021; Marshall 2010; World Health Organization (WHO) 2021) and the references therein, that the virus affects blood vessels, and therefore, the body organs, which may cause long term health complications. Currently, the pandemic affects all parts of the world, and can be found in over 200 countries and territories (Center for Systems Science and Engineering at Johns Hopkins University (JHU) 2021; World Health Organization (WHO) 2021; Worldometer 2021). The World Health Organization (WHO) declared COVID-19 a pandemic on 11 March 2020, which caused the introduction of emergency measures: large scale closing of borders, and lock-down of countries, states, regions, cities, and communities, as well as closing of schools and universities. As of 8 Aug. 2020, globally, there are over 14 million confirmed cases, over 600,000 deaths and over eight million recovered (Center for Systems Science and Engineering at Johns Hopkins University (JHU) 2021; Worldometer 2021). Thus, the number of COVID-19 infections by far exceed the number of SARS or the Middle East Respiratory Syndrome (MERS) infections. The SARS-CoV-2 human-to-human virus transmission is mainly via airborne fluid droplets, especially among those who are in close proximity. Transmission from infected patients to healthcare personnel has been often observed.

Because of the global impact of the pandemic, many researchers have been engaged in mathematical and statistical modeling of various aspects of the disease dynamics, aiming at predicting global and national trends, as well as specific regional behaviors of the virus spread. These are meant to help policymakers with hospital and emergency services preparedness and utilization; national and regional policy response decisions; business plans; implementation, relaxation and evaluation of various control measures; organization of large scale vaccination; and scientific understanding of the many facets of the disease dynamics. These efforts are reflected in the large number of relevant

publications listed in, see, e.g., (Centers for Disease Control and Prevention (CDC) 2020; Wikipedia 2020b; World Health Organization (WHO) 2021), and many recent publications such as (Anguelov et al. 2020; Eikenberry et al. 2020; Fanelli and Piazza 2020; Garba et al. 2020; Giordano et al. 2020; Hou et al. 2020). An interesting mathematical model dealing with some of the social implications of the pandemic is Johnston and Pell (2020). Since this work is concerned with simulations until 8 Aug. 2020, we do not consider new virus strains, or the global vaccination efforts that are underway.

We construct a new model for the COVID-19 pandemic to help researchers and policymakers evaluate the effectiveness and effects of various intervention and mitigation strategies, in real-time. It is based on the ideas underlying the MERS model in (Al-Asuoad 2017; Al-Asuoad and Shillor 2018; Al-Asuoad et al. 2016). However, our preliminary simulations of the COVID-19 pandemic using this MERS model produced unsatisfactory results. One of the main reasons is related to the government-mandated measures (how strict they were, how well they were communicated and enforced) and how well the population complied with them. Therefore, we distinguish those who follow properly the directives (wear masks in public, keep an appropriate distance from other people and frequently wash hands and/or use disinfectants) and those who do not or only partially do so. The latter group includes also health care personnel who have to be in contact with sick people, retirement homes' personnel, and other essential workers. To account for this, we introduce a new time-dependent parameter θ that represents the division of the exposed and infected subpopulations into those who fully comply and those who comply only partially. This parameter measures both the effectiveness of the directives and the population's compliance and allows to study the effects of these control measures and the possible impact of relaxing or tightening them on the disease spread. A related parameter in a simpler model was introduced in (Anguelov et al. 2020; Garba et al. 2020), where the focus was on estimating the size of the exposed but asymptomatic population. Our model provides this information, too.

The second novelty is in considering the 'adequate contact parameter' β , (Hethcote 2000), as one of the model dependent variables, instead of the usual assumption that it is a fixed constant, or a function of time, see e.g., (Greenhalgh and Das (2020); Greenhalgh and Day (2017); O'Neill (1997); Thieme and Yang (2002)) and the references therein. The case when β depends on the number of recovered R can be found in Báez-Sánchez and Bobko (2020), where it is shown how the choice of $\beta(R)$ affects the stability of the equilibrium points in a 'simple' SIR model. Here, instead of having to modify and fit β as the pandemic progressed, we consider it as a dependent variable, since it is known that β changes with changing population behavior, (Thieme (2003); Wikipedia (2021)), with tightened/relaxed control measures, seasonal changes, and availability of more information on the spread of COVID-19 and its effects on human health. The change in β can also be caused by the introduction of more effective face masks, and possible mutations. The latter will likely involve randomness that we would like to study in the future. Furthermore, in

simple SEIR models, there is a saturation phenomenon, that is, a decline in infectivity unrelated to the ‘herd immunity,’ see e.g., (Gai et al. 2020; Heesterbeek and Metz 1993; Zhang and Ma 2003) and references therein. By choosing β to be one of the model unknowns, we keep track of the intrinsic changes of the contact parameter, which includes the virus ‘infectiveness,’ and also the changes in human behavior. Since $1/\beta$ is the average number of contacts needed to infect a healthy person, it has a restricted range, $0 < \beta \leq 1$. This restriction is modeled by a differential inclusion. For the sake of simplicity, we assume that β grows (linearly) with the infected and decays (linearly) with the recovered. This linearity assumption is *ad-hoc* and is not based on any deeper epidemiological considerations. Therefore, it is of considerable interest to explore more appropriate forms of the inclusion in the future. Choosing β as an unknown that is described by a differential inclusion captures the evolution of the pandemic more naturally and is expected to make the model more accurate. However, our simulations for South Korea shows that β varies very little over the 175 days of simulations, so taking it as a fixed parameter, in this case, leads to very similar results. This is likely due to their successful COVID-19 containment and mitigation strategies. Nevertheless, long-time simulations (1,000 days) show that β changes to a lower value, which indicates that it is affected by the process. A third novelty is the theoretical introduction of randomness into the model parameters. This will be used in future works to study the sensitivity of the model to certain parameters and thus allowing for better predictions, as well as the introduction of virus mutations.

Since the model includes a differential inclusion, we establish the existence of the unique solution for the initial value problem, based on a theorem in abstract Hilbert spaces, (Brézis 1973). Moreover, the introduction of randomness into the model parameters raises the question of the measurability of the solutions with respect to the random variables. These mathematical issues are discussed in some detail in Sections 3 and 4.

An algorithm for the model simulations was constructed and implemented in MATLAB. Several simulations that show the predictive power of the model are presented in the context of the pandemic dynamics in the Republic of Korea. South Korea is chosen for the case study because it is one of the first countries to go through the disease cycle and the information provided by the government is very reliable. In the simulations, we use some of the published data to ‘train’ the model by using an optimization routine in MATLAB which finds the model parameters that provide a ‘best ℓ^1 fit.’ We present our simulated model predictions together with the data, one part of which (the first 100 days) was used in the optimization while the remaining 75 days depict how close the model predictions and the data are. The simulations of 175 days indicate that the model captures well the disease dynamics in South Korea.

Following this introduction, the mathematical model for the pandemic is constructed in Section 2. It consists of a coupled system of seven nonlinear ordinary differential equations and a differential inclusion for the contact variable β . The existence of the unique solution to the model is established in Section 3. Section 4 describes very briefly the addition of randomness and the

measurability of the solutions with random parameters. The stability of the two equilibrium states, the disease-free equilibrium (DFE) and the endemic equilibrium (EE), is presented in Section 5, based on an expression for the system's Jacobian derived in the Appendix. Section 6 outlines the algorithm used in the numerical simulations. Section 7 reports the results of the simulations of the COVID-19 dynamics in South Korea. The baseline simulations are in Subsection 7.1, where the model predictions are compared to the data. This section also provides additional information about the various subpopulations, which is difficult to obtain in the field, such as those who carry the virus, can infect others, but are undocumented and asymptomatic, and the variation in β as well as the stability of the DFE and EE. The effectiveness of the control measures and their connection to θ is studied in Subsection 7.2, while Subsection 7.3 presents the resulting case fatality and the infection fatality rates. Conclusions, unresolved issues and future work can be found in Section 8.

2 The Model

This section presents a mathematical model for the dynamics of the COVID-19 pandemic. It is based on the ideas that led to the MERS model in (Al-Asuoad 2017; Al-Asuoad and Shillor 2018; Al-Asuoad et al. 2016). However, there are significant differences between the compartmental structures and the resulting set of equations of the two models. In particular, this model separates the subpopulations of those who comply with the disease control directives and those who choose not to or partially comply.

The model describes whole populations and assumes that they are large enough to justify continuous dependent variables, thus, we use ordinary differential equations (ODEs). When the geographical distribution of the disease is important, or when the density and culture of the population vary in different parts of the country, it must be modified and partial differential equations (PDEs) need to be used instead. However, using PDEs considerably increases the mathematical complexity of the model and is beyond the scope of this work.

The model assumes that there may be various disease control measures such as voluntary or mandatory isolation, shelter-in-place directives, movement controls, closure of various public spaces and places, physical-distancing, and that a portion of the population practices these measures with varying degree. It describes the dynamics of seven subpopulations: *susceptibles* S ; *asymptomatic (exposed) fully compliant* E_{fc} ; *asymptomatic (exposed) partially compliant or noncompliant* E_{pc} ; *infected fully compliant*, I_{fc} ; *partially compliant or noncompliant infected* I_{pc} ; *hospitalized* H ; and *recovered* R . Unlike the usual SEIR models where those in the E compartment(s) are latent and cannot infect others, here the term 'exposed' also includes those who carry the virus and can infect others, but do not exhibit any symptoms. This compartment is of considerable interest in COVID-19 since a portion of the infections were caused by individuals in E . For the sake of simplicity, we refer below to partially com-

pliant or noncompliant as partially compliant. In addition, the model includes a differential inclusion for the infection rate function β . The populations and β are functions of time, which is measured in days. The compartmental structure of the model is depicted in Figure 1.

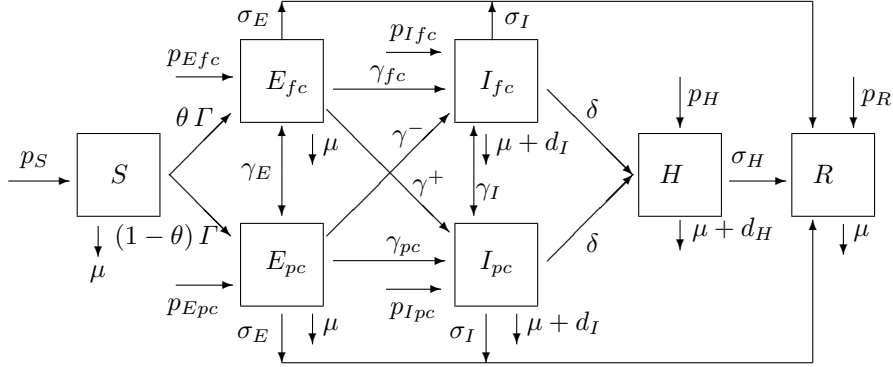


Fig. 1: Compartmental structure and flow chart for the COVID-19 model; μ is the natural death rate; p_S, \dots, p_R are influxes of individuals from outside; $\gamma_{fc}, \dots, \gamma_I$, are infection rates; δ is the hospitalization rate; $\sigma_E, \sigma_I, \sigma_H$ are recovery rates; and d_I, d_H are the disease death rates; Γ is the *force of infection* given in (9).

The susceptible subpopulation $S(t)$ consists of those who are healthy (only in terms of the COVID-19, while they may have other health conditions) and can become sick, or do not belong to any of the other groups. The subpopulations $E_{fc}(t)$ and $E_{pc}(t)$ denote the current numbers of those exposed to COVID-19 who fully comply with the disease control directives and those who do not or do so partially, respectively. The subpopulation $E_{pc}(t)$ includes also those who because of work or other circumstances cannot fully follow the shelter-in-place and the other directives. Furthermore, the subpopulations $E_{fc}(t)$ and $E_{pc}(t)$ consist of: asymptomatics – those who do not become sick; pre-symptomatics – those who in 5-14 days develop clinical symptoms; and those who do not show symptoms or are mildly symptomatic but are not tested and documented. It is established that both subpopulations carry the virus and can infect susceptibles and as noted above, they include the latent individuals who cannot infect others and also those who can.

The subpopulations $I_{fc}(t)$ and $I_{pc}(t)$ consist of documented infected individuals who are fully compliant or partially compliant, respectively, with no, mild, or medium clinical symptoms. $H(t)$ denotes those whose symptoms are severe or critical and are hospitalized. Finally, $R(t)$ denotes the individuals who recovered from COVID-19 and as of Aug. 2020, there are approximately 9 million such individuals in the world. We assume that recovered individuals have temporal immunity and cannot become infected again. Moreover, at this stage it is not known how long this immunity lasts. If evidence of reinfection

emerges, it is straightforward to modify the model to add reinfection pathways in the compartmental structure, possibly with delays.

Next, we define the parameters of the model. The total living population at time t is given by

$$N(t) = S(t) + E_{fc}(t) + E_{pc}(t) + I_{fc}(t) + I_{pc}(t) + H(t) + R(t).$$

We denote by $p_S(t)$ the number of susceptible individuals that are added each day by birth or by travel from outside of the region of interest. We let $p_{E_{fc}}(t)$ and $p_{E_{pc}}(t)$ be the per day influx of fully compliant and partially compliant exposed, respectively, and note that this influx (mostly by air travel) seems to be one of the main reasons why COVID-19 spread so quickly around the globe (see, e.g., (Nextstrain 2020)). Next, $p_{I_{fc}}(t)$ and $p_{I_{pc}}(t)$ denote the per day influxes of fully compliant infected and partially compliant infected populations, respectively. Then, $p_H(t)$ is the number of those who arrive sick on day t and need hospitalization, and $p_R(t)$ is the influx of recovered individuals.

The ‘natural’ death rate coefficient (in the absence of COVID-19) of the population, μ (1/day), can easily be obtained from the demographic information of the country and can be considered as given.

Next, the *contact rate* (or the infection rate coefficient) $\beta(t)$ (1/day) at time t is the average number of contacts sufficient for transmission. The rates of infection of a susceptible by a fully or partially compliant asymptomatic, a fully or partially compliant infected, or a hospitalized results in infection, respectively, are

$$\epsilon_{E_{fc}}\beta, \quad \epsilon_{E_{pc}}\beta, \quad \epsilon_{I_{fc}}\beta, \quad \epsilon_{I_{pc}}\beta, \quad \epsilon_H\beta,$$

(1/day). The ϵ 's are nonnegative dimensionless infection rate modification constants. When the isolation is very effective, the first and the last three are likely to be small, since contacts are discouraged, and ϵ_H should be kept small in every hospital environment.

The rate Γ , the so-called *force of infection*, is given by

$$\Gamma = \frac{\beta}{N}(\epsilon_{E_{fc}}E_{fc} + \epsilon_{E_{pc}}E_{pc} + \epsilon_{I_{fc}}I_{fc} + \epsilon_{I_{pc}}I_{pc} + \epsilon_H H),$$

and measures the rate at which susceptibles get infected. We note that to model the case when E represents only those that are latent and cannot infect others, one has to set $\epsilon_{E_{fc}} = \epsilon_{E_{pc}} = 0$. The rate, per day, at which the fraction θ of the susceptibles becomes exposed fully compliant is $\theta\Gamma S$, and the rest becomes exposed partially compliant at the rate $(1 - \theta)\Gamma S$. Moreover, we allow fully compliant exposed to become partially compliant exposed and vice versa, with rate constant γ_E . This may be triggered by a change in their views or their economic situation. The rate constant γ_I has a similar interpretation. The parameters γ_{fc}, γ_{pc} (1/day) denote the rate constants of development of clinical symptoms in fully compliant and partially compliant exposed individuals, while γ^-, γ^+ are the rate constants of clinical symptoms in fully compliant who become partially compliant and infected (hopefully small), and those

partially compliant exposed who become fully compliant infected. The model assumes that there is no disease-induced death in the exposed populations. Next, the rate constant at which the fully compliant infected and the partially compliant infected individuals need hospitalization is assumed to be the same, δ . The additional disease-induced death for the infected and hospitalized are d_I and d_H , respectively. To complete the flow chart, we denote by σ_E, σ_I and σ_H the recovery rates of the exposed, infected and hospitalized, respectively.

Finally, the model takes into account the changes in the contact number, which also includes the virulence (infectivity) and other effects related to changes in contact, of the coronavirus via a novel differential inclusion for the infection rate coefficient β . These changes may be due to the changes in social behavior, changes in weather (allowing more people to be outside where the infection rates are smaller), or minor mutations of the virus. We assume that β increases in proportion to the infected population, with rate coefficient $\delta_* \geq 0$, and decreases in proportion to the population immunity and the number of those recovered, with rate constant $\delta^* \geq 0$. This is expressed in the differential inclusion (10) and a detailed explanation can be found below. However, this differential inclusion is *ad-hoc* and different formulations will be investigated in the future when a deeper understanding of the virus dynamics emerges. Moreover, it may be of interest to add in the future the effects of vaccination.

With the notation and assumptions given above, our model for the COVID-19 pandemic is defined below.

Model 1 Find eight functions $(S, E_{fc}, E_{pc}, I_{fc}, I_{pc}, H, R, \beta)$, defined on $[0, T]$, that satisfy the following system of ODEs,

$$\frac{dS}{dt} = p_S - \Gamma S - \mu S, \quad (1)$$

$$\frac{dE_{fc}}{dt} = p_{E_{fc}} + \theta \Gamma S - \left(\gamma_{fc} + \gamma^+ + \sigma_E + \mu - \frac{\gamma_E}{N} E_{pc} \right) E_{fc}, \quad (2)$$

$$\frac{dE_{pc}}{dt} = p_{E_{pc}} + (1 - \theta) \Gamma S - \left(\gamma_{pc} + \gamma^- + \sigma_E + \mu + \frac{\gamma_E}{N} E_{fc} \right) E_{pc}, \quad (3)$$

$$\frac{dI_{fc}}{dt} = p_{I_{fc}} + \gamma_{fc} E_{fc} + \gamma^- E_{pc} - \left(\delta + \sigma_I + d_I + \mu - \frac{\gamma_I}{N} I_{pc} \right) I_{fc}, \quad (4)$$

$$\frac{dI_{pc}}{dt} = p_{I_{pc}} + \gamma_{pc} E_{pc} + \gamma^+ E_{fc} - \left(\delta + \sigma_I + d_I + \mu + \frac{\gamma_I}{N} I_{fc} \right) I_{pc}, \quad (5)$$

$$\frac{dH}{dt} = p_H + \delta(I_{fc} + I_{pc}) - (\sigma_H + d_H + \mu)H, \quad (6)$$

$$\frac{dR}{dt} = p_R + \sigma_E(E_{fc} + E_{pc}) + \sigma_I(I_{fc} + I_{pc}) + \sigma_H H - \mu R, \quad (7)$$

$$N = S + E_{fc} + E_{pc} + I_{fc} + I_{pc} + H + R, \quad (8)$$

$$\Gamma = \frac{\beta}{N} (\epsilon_{E_{fc}} E_{fc} + \epsilon_{E_{pc}} E_{pc} + \epsilon_{I_{fc}} I_{fc} + \epsilon_{I_{pc}} I_{pc} + \epsilon_H H), \quad (9)$$

$$\frac{d\beta}{dt} = \delta_* \Gamma - \delta^* \beta \frac{R}{N} - \zeta, \quad \zeta \in \partial I_{[\beta_*, \beta^*]}(\beta), \quad (10)$$

together with the initial conditions,

$$\begin{aligned} S(0) &= S_0, E_{fc}(0) = E_{fc0}, E_{pc}(0) = E_{pc0}, I_{fc}(0) = I_{fc0}, I_{pc}(0) = I_{pc0}, \\ H(0) &= H_0, R(0) = R_0, \\ \beta(0) &= \beta_0 \in [\beta_*, \beta^*]. \end{aligned} \tag{11}$$

Here, $S_0 > 0$ is the initial population at the breakout of the pandemic; $E_{fc0}, E_{pc0}, I_{fc0}, I_{pc0}, H_0$ and R_0 are nonnegative initial subpopulations, and β_0 is the initial transmission rate which can be estimated from the data.

In practice, one typically assumes that $S_0 = N(0) > 0$, so that at the start of the pandemic there are only susceptibles, and all the other populations vanish. However, for the sake of generality, we allow initially the other subpopulations to be nonnegative. Specifically, if the starting point is later than the very first day of the pandemic,

$$N(0) = S_0 + E_{fc0} + E_{pc0} + I_{fc0} + I_{pc0} + H_0 + R_0,$$

so that (8) holds initially. A summary of the definitions of the model parameters is given in Table 1.

Equation (1) describes the rate of change, per day, of the susceptible population. The second term on the right-hand side is the rate at which the susceptibles become infected by contact with exposed, infected, and hospitalized individuals. We emphasize that the exposed populations include the asymptomatics that may cause infection. The last term describes the ‘natural’ (unrelated to the pandemic) mortality.

The rest of the equations, except (10), have a similar structure and interpretation. For instance, in (6) the rate of change, per day, of the hospitalized is the sum of those who arrive from outside (say overflow in other locations), p_H , and fully compliant and partially compliant infectives whose illness becomes severe and need hospitalization, $\delta(I_{fc} + I_{pc})$, minus those who recovered on that day, $\sigma_H H$, those who died naturally, μH , and those who died because of the pandemic, $d_H H$.

We note that in our model, the usual expression for the probability that one susceptible is infected (per day), $\beta I/N$, is replaced with Γ . This means that the values of β must be restricted, which we describe next.

Next, we describe equation (10), actually a differential inclusion, for the change in the infectiveness of the SARS-CoV-2 virus. We assume a ‘simple’ linear relationship between the infection rate coefficient β and the fractions of those who carry the virus and the recovered. In particular, an increase in the fraction who have the virus and can infect others, $(E_{fc} + E_{pc} + I_{fc} + I_{pc} + H)/N$, is assumed to make the virus more infective, while an increase in the fraction of recovered, R/N , is assumed to increase the immunity of the population leading to a decrease in the disease virulence. Finally, we use a subdifferential (explained below) to guarantee that β remains in the admissible set $[\beta_*, \beta^*]$, where β_* and β^* are appropriate values such that $0 \leq \beta_* < \beta^*$. Let $I_{[\beta_*, \beta^*]}(\beta)$ be the indicator function of the interval $[\beta_*, \beta^*]$, which vanishes when β is

in the interval and has the value $+\infty$, otherwise. Then, its subdifferential, $\partial I_{[\beta_*, \beta^*]}(\beta)$, is the set-valued function or multifunction

$$\partial I_{[\beta_*, \beta^*]}(\beta) = \begin{cases} (-\infty, 0] & \text{if } \beta = \beta_*, \\ 0 & \text{if } \beta_* < \beta < \beta^*, \\ [0, \infty) & \text{if } \beta = \beta^*, \\ \emptyset & \text{otherwise.} \end{cases} \quad (12)$$

Adding this term guarantees that $\beta_* \leq \beta(t) \leq \beta^*$ for $0 \leq t \leq T$. Indeed, when $\beta \in (\beta_*, \beta^*)$ then $\zeta = 0$ and (9) is just a rate equation. When $\beta(t) = \beta_*$ then there exists an element $-\zeta \in [0, \infty)$ that prevents β from becoming smaller than β_* ; and when $\beta(t) = \beta^*$ there exists an element $-\zeta \in (-\infty, 0]$ that prevents β from exceeding β^* .

The number of active ‘documented’ or identified cases $A(t)$, at time t , is

$$A(t) = I_{fc}(t) + I_{pc}(t) + H(t),$$

and, following (Worldometer 2021), we denote by $A_m(t) = I_{fc}(t) + I_{pc}(t)$ and $A_c(t) = H(t)$ those with an active mild condition, documented but not serious, which can be with no symptoms, mild or medium symptoms, and those with serious or critical conditions, respectively.

Next, $CC(t)$, the cumulative or total number of cases, up to time t , is

$$CC(t) = A(t) + CR(t) + CD(t), \quad (13)$$

where the cumulative number of the recovered CR is given by

$$CR(t) = R_0 + \int_0^t \left(\sigma_E (E_{fc}(\tau) + E_{pc}(\tau)) + \sigma_I (I_{fc}(\tau) + I_{pc}(\tau)) + \sigma_H H(\tau) \right) d\tau;$$

the daily number of deaths caused by the disease is

$$D(t) = d_I (I_{fc}(t) + I_{pc}(t)) + d_H H(t);$$

and the cumulative or total number of deaths $CD(t)$ caused by the disease is

$$CD(t) = D_0 + \int_0^t D(\tau) d\tau. \quad (14)$$

The number of new cases on day t is given by

$$C_{day}(t) = CC(t) - CC(t-1). \quad (15)$$

Finally, the cumulative number $CA(t)$ of those who recovered from the asymptomatic population is given by

$$CA(t) = \sigma_E \int_0^t (E_{fc}(\tau) + E_{pc}(\tau)) d\tau, \quad (16)$$

assuming that the initial number of the asymptomatic who recovered is zero.

In this way, the model provides insight into an important aspect of the pandemic that is very difficult to obtain in the field.

3 Existence and uniqueness of the solution

Proving the existence of a unique solution to the model for each finite time interval is a mathematically important next step. Without the differential inclusion (10) and when θ is a known continuous and bounded function, the local existence in time follows from the fact that the functions on the right-hand sides of the equations are locally Lipschitz. Then, the existence of the global solution is established by demonstrating that the solution stays bounded on every finite time interval. This includes showing that given nonnegative initial conditions, the solution components stay nonnegative, which is not only necessary mathematically but also important for the model to be biologically relevant. However, this is not the case in our model. Specifically, we allow θ to be bounded and piecewise continuous, hence not continuous, and β is not given but a solution of a differential inclusion. Therefore, the standard way outlined above no longer works, requiring a more sophisticated approach that we detail in what follows.

We assume that the input functions $p_S(t), \dots, p_R(t)$ are bounded, nonnegative, and smooth and all the parameters, except for γ_E and γ_I , are positive constants.

First, we assume that $\theta(t)$ is given and $0 \leq \theta(t) \leq 1$ for all $t \in [0, T]$, and β is a given smooth function with values in $[\beta_*, \beta^*] \subset (0, 1]$. Below, we relax the assumption that β is given.

Positivity of $E_{fc}; E_{pc}; I_{fc}; I_{pc}; H; R$. We first establish the non-negativity of the solutions of the system when the initial data is non-negative (except for $S_0 > 0$). To that end, let $S_0 > 0$ and assume that the other initial conditions satisfy $E_{fc0}, E_{pc0}, I_{fc0}, I_{pc0}, H_0, R_0 \geq \varepsilon > 0$, and also $p_R \geq \varepsilon$. Below, we let $\varepsilon \rightarrow 0$. Thus, there exists $T_1 > 0$, which we may assume to be the largest time, such that the local solution exists and is unique on $[0, T_1)$. The continuity of the solution implies that there is a maximal time t_* , satisfying $0 < t_* \leq T_1$, which may depend on ε , such that the solution is component-wise positive on $[0, t_*)$. Moreover, we have that $N > 0$ on $[0, t_*]$, since otherwise if $N(t_*) = 0$ then by (8),

$$S(t_*) = E_{fc}(t_*) = E_{pc}(t_*) = I_{fc}(t_*) = I_{pc}(t_*) = H(t_*) = R(t_*) = 0,$$

and it follows from (7) that at $t = t_*$,

$$\frac{dR}{dt} \geq \varepsilon > 0,$$

which means that R is an increasing function at t_* , and since $R(t) > 0$ on $[0, t_*)$, it is positive on $[0, t_*]$, and then $N > 0$ on $[0, t_*]$.

Then (9) implies that

$$0 \leq \Gamma < 5\beta^* \max(\epsilon_{E_{fc}}, \epsilon_{E_{pc}}, \epsilon_{I_{fc}}, \epsilon_{I_{pc}}, \epsilon_H) := \Gamma^*, \quad (17)$$

since $E_{fc}, E_{pc}, I_{fc}, I_{pc}, H < N$ and $\beta \leq \beta^*$ on $[0, t_*]$. It follows from (1) that

$$\frac{dS}{dt} \geq p_S - (\Gamma^* + \mu)S,$$

on $[0, t_*]$. Since $S_0 > 0$ and $p_S \geq 0$, then on $[0, t_*]$,

$$S(t) \geq S_0 \exp(-(\Gamma^* + \mu)t) \geq S_0 \exp(-(\Gamma^* + \mu)t_*) > 0.$$

Next, we introduce the following notation for the sake of simplicity,

$$\widehat{\gamma}_{fc} := \gamma_{fc} + \gamma^+ + \sigma_E + \mu, \quad (18)$$

$$\widehat{\gamma}_{pc} := \gamma_{pc} + \gamma^- + \sigma_E + \mu, \quad (19)$$

$$\widehat{\delta} := \delta + \sigma_I + d_I + \mu, \quad (20)$$

and assume that the parameters satisfy

$$|\gamma_E| < \min\{\widehat{\gamma}_{fc}, \widehat{\gamma}_{pc}\}, \quad |\gamma_I| < \widehat{\delta}, \quad (21)$$

which is necessary to prove boundedness but also makes the model biologically relevant.

Next, we consider (2) and since $\theta \Gamma S \geq 0$ and $E_{pc} < N$, we obtain

$$\frac{dE_{fc}}{dt} \geq p_{E_{fc}} - (\widehat{\gamma}_{fc} + |\gamma_E|)E_{fc},$$

and since $p_{E_{fc}} \geq 0$, we find that $E_{fc}(t) \geq E_{fc0} \exp(-(\widehat{\gamma}_{fc} + |\gamma_E|)t_*) > 0$ on $[0, t_*]$. We now consider (3), and since $p_{E_{pc}} \geq 0$, $(1 - \theta)\Gamma S \geq 0$ and $E_{fc} < N$, we have

$$\frac{dE_{pc}}{dt} \geq p_{E_{pc}} - (\widehat{\gamma}_{pc} + |\gamma_E|)E_{pc},$$

therefore, $E_{pc}(t) \geq E_{pc0} \exp(-(\widehat{\gamma}_{pc} + |\gamma_E|)t_*) > 0$ on $[0, t_*]$.

The arguments concerning (4) and (5) are similar. Since $p_{I_{fc}} \geq 0$, by omitting all the nonnegative terms in (4), we find,

$$\frac{dI_{fc}}{dt} \geq p_{I_{fc}} - (\widehat{\delta} + |\gamma_I|)I_{fc},$$

and hence, $I_{fc}(t) \geq I_{fc0} \exp(-(\widehat{\delta} + |\gamma_I|)t_*) > 0$ on $[0, t_*]$. Similarly, it follows from (5) that $I_{pc}(t) \geq I_{pc0} \exp(-(\widehat{\delta}_{fc} + |\gamma_I|)t_*) > 0$ on $[0, t_*]$.

We turn to (6). Since $p_H \geq 0$ and $\delta_{fc}I_{fc} + \delta_{pc}I_{pc} > 0$, we have

$$\frac{dH}{dt} \geq -(\sigma_H + d_H + \mu)H,$$

and so $H(t) \geq H_0 \exp(-(\sigma_H + d_H + \mu)t_*) > 0$ on $[0, t_*]$. Finally, it follows from (7) that

$$\frac{dR}{dt} > -\mu R,$$

and hence $R(t) > R_0 \exp(-\mu t_*) > 0$ on $[0, t_*]$.

We note that all the decay rates in the estimates above depend on the problem data but are independent of ε , then all the variables $S(t), \dots, R(t)$, as well as $N(t)$ and $\Gamma(t)$, are positive on the closed interval $[0, t_*]$, and since the solution is continuous, we conclude that they are strictly positive on $[0, T_*]$ for some $t_* < T_* < T_1$, and by extension $T_* = T_1$. Indeed, if $S(t_*) = \alpha_S > 0$ and S is defined and continuous at t_* , then there exists an interval $(t_* - \xi, t_* + \xi)$, for some $\xi > 0$, such that $S(t) \geq \alpha_S/2$ on $(t_* - \xi, t_* + \xi)$.

We conclude that when $\varepsilon > 0$, i.e., the initial conditions are positive, then the solution is positive as long as it exists. However, it is noted that T_* does not depend on ε , and therefore, we have the following summary.

Proposition 1 *Assume that (21) holds, $S_0 > 0$, the other initial conditions are nonnegative, and θ and β are bounded and positive. Then, the solution of system (1)-(7) is positive as long as it exists.*

Now that it is established that under the assumptions of Proposition 1, the solution is positive as long as it exists, the only way it can cease to exist is when one or more of the variables approaches infinity in finite time.

Boundedness of $S, E_{fc}, E_{pc}, I_{fc}, I_{pc}, H, R$ on finite intervals In the second step, under the assumptions of Proposition 1, we show that each of $S(t), \dots, R(t)$ is bounded on every finite time interval, and therefore, the solution cannot approach infinity in finite time. This is sufficient to show that the solution exists on each finite time interval. We begin with the interval of existence, $[0, T_1)$.

We note that since $p_S(t)$ is bounded and $\Gamma > 0$, equation (1) shows that $S(t)$ is bounded on every finite time interval it exists on. Using the definition of $\hat{\gamma}_1$ given by (18) in equation (2), $0 \leq \theta \leq 1$, the bound on Γ given by (17), and $0 < E_{pc}/N < 1$, yield

$$\frac{dE_{fc}}{dt} < p_{E_{fc}} + \Gamma^* S - (\hat{\gamma}_{fc} - |\gamma_E|)E_{fc}.$$

Then, by assumption (21) that $|\gamma_E| < \hat{\gamma}_{fc}$ and since $p_{E_{fc}}$ and S are bounded, it follows that E_{fc} is bounded. We now consider (3). Using the definition of $\hat{\gamma}_{pc}$ given by (19), $0 \leq 1 - \theta \leq 1$, and (17),

$$\frac{dE_{pc}}{dt} < p_{E_{pc}} + \Gamma^* S - (\hat{\gamma}_{pc} - |\gamma_E|)E_{pc}.$$

Since $p_{E_{pc}}$ and S are bounded and $\hat{\gamma}_{pc} > |\gamma_E|$, it follows that E_{pc} is bounded. Next, using the definition of $\hat{\delta}$ from (20) and $0 < I_{pc}/N < 1$ in (4) and (5), we obtain

$$\begin{aligned} \frac{dI_{fc}}{dt} &< p_{I_{fc}} + \gamma_{fc}E_{fc} + \gamma^- E_{pc} - (\hat{\delta} - |\gamma_I|)I_{fc}, \\ \frac{dI_{pc}}{dt} &< p_{I_{pc}} + \gamma_{pc}E_{pc} + \gamma^+ E_{fc} - (\hat{\delta} - |\gamma_I|)I_{pc}. \end{aligned}$$

Since $|\gamma_I| < \hat{\delta}$, (21), and $p_{I_{fc}}, p_{I_{pc}}, E_{fc}$ and E_{pc} are all bounded, the boundedness of I_{fc} and I_{pc} follows. The boundedness of H and R follows directly

from equations (6), (7) and the fact that p_H, p_R and $E_{fc}, E_{pc}, I_{fc}, I_{pc}$ are all bounded independently of the choice of $\beta \in [\beta_*, \beta^*]$.

We summarize the result as follows.

Proposition 2 *Assume that $S_0 > 0$, the other initial conditions are nonnegative, and θ and β are bounded and positive. Moreover, assume that*

$$|\gamma_E| < \min\{\widehat{\gamma}_{fc}, \widehat{\gamma}_{pc}\}, \quad |\gamma_I| < \widehat{\delta}.$$

Then, the solution of system (1)-(7) is positive and bounded on every finite interval.

Before proceeding with the existence proof, we note that $\Gamma(t)$ is bounded and positive and the boundedness results above and equation (8) imply that $N(t)$ is bounded and positive on every finite interval. Furthermore, the differential set-inclusion (10) can be rewritten as

$$\frac{d\beta}{dt} + \delta^* \frac{R}{N} \beta + \partial\phi(\beta) \ni \delta_* \Gamma, \quad \beta(0) = \beta_0 \in [\beta_*, \beta^*], \quad (22)$$

where $\phi(\beta) = I_{[\beta_*, \beta^*]}(\beta)$, and $\partial\phi(\beta)$ is its subdifferential, (12). Since ϕ in (22) is convex and lower semicontinuous, its subdifferential $\partial\phi$ forces β to remain in the interval $[\beta_*, \beta^*]$.

Existence and uniqueness To use the powerful tools of convex analysis for the existence and uniqueness proof, we first reformulate the problem in an abstract form. Letting

$$\mathbf{x} = (S, E_{fc}, E_{pc}, I_{fc}, I_{pc}, H, R),$$

the system defined by equations (1)-(7) together with (8) and (9), can be written as

$$\mathbf{x}' = \mathbf{F}(t, \mathbf{x}, \beta, \theta), \quad \mathbf{x}(0) = \mathbf{x}_0, \quad (23)$$

where \mathbf{F} is Lipschitz in \mathbf{x}, β and θ ; β is a given continuous function having values in $[\beta_*, \beta^*]$; and θ and is bounded with values in $[0, 1]$.

We first assume that θ is continuous. Below, we relax this assumption and allow it to be piecewise continuous. Let β and $\hat{\beta}$ be two continuous functions such that $\beta(t), \hat{\beta}(t) \in [\beta_*, \beta^*]$ for all $t \in [0, T]$. We let \mathbf{x} and $\hat{\mathbf{x}}$ be the solutions to (23) corresponding to β and $\hat{\beta}$, respectively. Then, using straightforward computations, as in (Hale 2009; Kuttler 2017; Richard Bellman 1995), we obtain a constant $C > 0$, independent of β and $\hat{\beta}$, such that

$$\begin{aligned} |\mathbf{x}(t) - \hat{\mathbf{x}}(t)|^2 &\leq C \int_0^t |\mathbf{F}(s, \mathbf{x}, \beta) - \mathbf{F}(s, \hat{\mathbf{x}}, \hat{\beta})|^2 ds \\ &\leq 2C \int_0^t \left(|\mathbf{F}(s, \mathbf{x}, \beta) - \mathbf{F}(s, \mathbf{x}, \hat{\beta})|^2 + |\mathbf{F}(s, \mathbf{x}, \hat{\beta}) - \mathbf{F}(s, \hat{\mathbf{x}}, \hat{\beta})|^2 \right) ds \\ &\leq 2CK^2 \int_0^t \left(|\beta - \hat{\beta}|^2 + |\mathbf{x} - \hat{\mathbf{x}}|^2 \right) ds. \end{aligned}$$

Here, K is an appropriate Lipschitz constant that depends on the estimates obtained above. Then, an application of Grönwall's inequality shows that after modifying the constants,

$$|\mathbf{x}(t) - \hat{\mathbf{x}}(t)|^2 \leq CK^2 \int_0^t |\beta - \hat{\beta}|^2 ds. \quad (24)$$

The Lipschitz continuity of \mathbf{F} ensures the existence and uniqueness of a solution to the initial value problem with given β and continuous θ (see e.g., Theorem 2.4 (Boyce and DiPrima 1986)).

We summarize the result of the discussion above as follows.

Proposition 3 *Assume that β is a continuous function having values in $[\beta_*, \beta^*]$. Then, there exists a unique solution to the initial value problem defined by (1)–(7), together with (8) and (9), and the initial conditions (11). Moreover, if $\mathbf{x}, \hat{\mathbf{x}}$ are two solutions corresponding to β and $\hat{\beta}$, then (24) holds for a constant C that is independent of β .*

Now, let $\beta \in C([0, T])$ such that $\beta(t) \in [\beta_*, \beta^*]$ for all t . Then, we use the solution that exists by Proposition 3 to construct a solution to the evolution inclusion (22), based on the following well-known theorem of Brézis (Brézis 1973). In our case the Hilbert space is \mathbb{R} and we assume that $\beta_0 \in [\beta_*, \beta^*]$.

Theorem 2 *Let H be a Hilbert space. Let $f \in L^2(0, T; H)$. Let ϕ be a lower semicontinuous convex proper function defined on H and β_0 be in the domain of ϕ . Then, there exists a unique solution $\beta \in L^2(0, T; H)$, $\beta' \in L^2(0, T; H)$, to*

$$\beta'(t) + \partial\phi(\beta(t)) \ni f(t) \quad a.e. t, \quad \beta(0) = \beta_0.$$

We also have the following result:

Corollary 1 *In addition to the assumptions of Theorem 2, suppose $f(t)$ is replaced with $f(t)\beta$, where $f \in L^\infty(0, T; H)$. Then, there exists a unique solution to the resulting inclusion.*

Proof Let $\hat{\beta} \in C([0, T]; H)$ and let $F(\hat{\beta})$ be the solution of

$$\beta'(t) + \partial\phi(\beta(t)) \ni f(t)\hat{\beta}. \quad (25)$$

Then, standard manipulations and the monotonicity of the subgradient, for $F(\hat{\beta})$ and $F(\bar{\beta})$, yield

$$\frac{1}{2}|(F(\hat{\beta}) - F(\bar{\beta}))(t)|_H^2 \leq \int_0^t \left(f(s)(\hat{\beta}(s) - \bar{\beta}(s)), (F(\hat{\beta}) - F(\bar{\beta}))(s) \right) ds.$$

This implies,

$$|(F(\hat{\beta}) - F(\bar{\beta}))(t)|_H^2 \leq C \int_0^t |\hat{\beta}(s) - \bar{\beta}(s)|^2 ds$$

and shows that a sufficiently high power of F is a contraction map. Hence, F has a unique fixed point that is the unique solution of the evolution inclusion (25).

Now, we turn to the whole problem defined by (1)–(11) and construct a mapping $\Theta : C([0, T]) \rightarrow C([0, T])$ as follows. Let $\bar{\beta} \in C([0, T])$ having values in $[\beta_*, \beta^*]$. Then, it follows from Proposition 3 that the solution to the initial value problem for such fixed $\bar{\beta}$ is unique. Now, we define a map $\Theta : C([0, T]) \rightarrow C([0, T])$ where $\Theta(\bar{\beta}) = \beta$, is the solution of (22) for the given $\bar{\beta}$. We write the equation for β , given $\bar{\beta}$, as

$$\frac{d\beta}{dt} + \delta^* \frac{R(\bar{\beta})}{N(\bar{\beta})} \beta + \partial\phi(\beta) \ni \delta_* \beta F(\bar{\beta}), \quad \beta(0) = \beta_0 \in [\beta_*, \beta^*].$$

Since the estimates above do not depend on the choice of $\bar{\beta}$, as long as it has values in $[\beta_*, \beta^*]$, the differential inclusion is of the form

$$\frac{d\beta}{dt} + \partial\phi(\beta) \ni G(t, \bar{x}, \bar{\beta}), \quad \beta(0) = \beta_0 \in [\beta_*, \beta^*],$$

where \bar{x} is the solution to the initial value problem with given $\bar{\beta}$, and G is a Lipschitz continuous function in both \bar{x} and $\bar{\beta}$.

To proceed, we let $\bar{\beta}_1$ and $\bar{\beta}_2$ be given with the properties as above, and let $\Theta(\bar{\beta}_1) \equiv \beta_1$ and $\Theta(\bar{\beta}_2) \equiv \beta_2$. Then, it follows from the inclusion and the monotonicity of $\partial\phi$ and routine computations that there exists a constant $C > 0$, independent of β and a suitable Lipschitz constant K , such that

$$\frac{1}{2} |\beta_1(t) - \beta_2(t)|^2 \leq 2CK^2 \int_0^t (|\bar{\beta}_1 - \bar{\beta}_2|^2 + |\bar{x}_1 - \bar{x}_2|^2) ds.$$

It follows from (24), after modifying the constants, that

$$\begin{aligned} |\Theta(\bar{\beta}_1)(t) - \Theta(\bar{\beta}_2)(t)|^2 &\equiv |\beta_1(t) - \beta_2(t)|^2 \\ &\leq C \left(\int_0^t (|\bar{\beta}_1 - \bar{\beta}_2|^2 ds + \int_0^t \int_0^s |\bar{\beta}_1(\tau) - \bar{\beta}_2(\tau)|^2 d\tau ds \right). \end{aligned}$$

Therefore, a sufficiently high power of Θ is a contraction mapping, and it has a unique fixed point that is the solution to the problem. This completes the proof of the existence and uniqueness of the solution of the full problem assuming the given function θ is continuous.

To take into account a piecewise continuous θ , we assume that there are finitely many non-overlapping time intervals $\{I_i\}$ and continuous functions $\theta_i(t)$ defined on \bar{I}_i such that $\theta(t) = \theta_i(t)$ on the interior of I_i . Then, on each interval where θ is continuous, we have a unique solution obtained as above, and it is straightforward to piece these into a global solution of the problem.

This leads to the main mathematical result in this work.

Theorem 3 *Assume that θ is bounded and piecewise continuous and*

$$|\gamma_E| < \min\{\hat{\gamma}_{fc}, \hat{\gamma}_{pc}\}, \quad |\gamma_I| < \hat{\delta}, \quad (26)$$

where $\hat{\gamma}_{fc}$, $\hat{\gamma}_{pc}$, $\hat{\gamma}_{fc}$ are defined as in (18)–(20). Then, there exists a unique solution to problem (1)–(11) on every finite time interval $[0, T]$.

We note that in the model the assumptions on γ_E and γ_I make sense, although it is possible to remove them at the expense of considerable additional effort in obtaining the estimates.

Finally, since β has values in $[\beta_*, \beta^*]$ and its derivative is in $L^2(0, T)$, it follows that β is Hölder continuous with exponent $1/2$. Therefore, the solution is at least in $C^{1,1/2}(0, T)$. It seems plausible that the regularity is higher since $\beta' \in L^\infty(0, T)$ and then it is Hölder continuous with exponent 1, however, we leave the question open as part of further study of the solution's regularity.

4 Randomness in system parameters

For the sake of completeness, this short section provides a rather abstract discussion about adding randomness to the system parameters. This allows a better understanding of the model's dependence on the parameter values. Moreover, to use the model as a predictive tool, it is crucial to find out how parameter changes affect model predictions. Small changes in the solution that are caused by small changes in a parameter indicate that there is low sensitivity to the parameter and an approximate value is sufficient for acceptable predictions, while considerable changes in the solution caused by small changes in the parameter values indicate that a more precise parameter value is needed to obtain reliable predictions. It may also indicate that the model is unstable or the process itself is unstable, in which case attempts at prediction may be of little use.

We now introduce randomness into the system parameters. For the sake of generality, we note that we have 38 system parameters including the 7 initial conditions, as listed in Table 1 and let the *probability space* be (Ω, \mathcal{F}, P) , where Ω is the *sample space*, a box centered at the origin of \mathbb{R}^{38} ; \mathcal{F} is the Borel σ -algebra, and P is a general probability function. We let $\bar{\omega} \in \Omega$ be the random variable and define

$$\omega = \hat{\omega} + \bar{\omega}, \quad (\omega \in \hat{\omega} + \Omega),$$

where $\hat{\omega}$ denotes the vector containing the optimized parameters. We note that the choice of Ω is such that $\omega \geq 0$ (component-wise).

Next, we consider the modified system (1)–(9) and (11), in the form

$$\mathbf{x}' = \mathbf{F}(t, \mathbf{x}, \beta, \omega), \quad \mathbf{x}_0(0) = \hat{\mathbf{x}}(\omega),$$

where $\hat{\mathbf{x}}(\omega) = \mathbf{x}_0 + \bar{\omega}$, $\bar{\omega} \in \Omega$, together with the differential inclusion

$$\frac{d\beta}{dt} + \tilde{\delta}^* \frac{R(\omega)}{N(\omega)} \beta + \partial\phi(\beta) \ni \delta_* \Gamma(\omega), \quad \beta(0) = \beta_0 \in [\beta_*, \beta^*].$$

Here, $\partial\phi(\beta) = I_{[\beta_*, \beta^*]}(\beta)$ is defined by (12). The function \mathbf{F} depends on ω such that $\omega \rightarrow \mathbf{F}(t, \mathbf{x}, \beta, \omega)$ is measurable, \mathbf{F} is Lipschitz continuous in \mathbf{x} and β and is continuous in all of the first three variables.

It follows from the recent results in (Kuttler et al. 2016) that the uniqueness of the solutions for each fixed ω implies that the functions $\omega \rightarrow \mathbf{x}(\cdot, \omega), \omega \rightarrow$

$\beta(\cdot, \omega)$ and $\omega \rightarrow \mathbf{F}(\cdot, \mathbf{x}(\cdot, \omega), \beta(\cdot, \omega), \omega)$ are each measurable into $C([0, T])$. Moreover, $\omega \rightarrow \beta'(\cdot, \omega)$ is measurable into $L^2(0, T)$, and then it follows from Theorem 3.3 in (Kuttler et al. 2016) that $(t, \omega) \rightarrow \beta'(t, \omega)$ can be considered as a product measurable function.

5 Stability of the DFE and the EE

This section discusses the stability of the critical points of the system: the disease-free equilibrium (DFE) and the endemic equilibrium (EE) (when it exists), based on the system's Jacobian matrix. The usual approach, see e.g., (Allen 2007; Hethcote 2000; Thieme 2003), is to derive the *basic stability number* \mathcal{R}_C . In simple SEIR models, \mathcal{R}_C coincides with the basic reproduction number R_0 , however, in more complex models the expression is naturally as complex as the model. When $\mathcal{R}_C < 1$, all the eigenvalues of the Jacobian, evaluated at the DFE, have negative real parts, which indicates that the DFE is asymptotically stable (i.e., stable and attracting), and there is no EE. On the other hand, $\mathcal{R}_C = 1$ is a bifurcation point, and when $\mathcal{R}_C > 1$ at least one of the real parts is positive and the DFE loses its stability. Usually, when the DFE becomes unstable the EE appears and is stable and attracting. However, because of the complexity of our model, we did not find a closed-form expression for \mathcal{R}_C , so, instead, we derived the Jacobian of the system (Appendix A) assuming that β is constant and evaluated it numerically at the DFE.

To proceed, we assume that $\beta = \beta_0 \in [\beta_*, \beta^*]$ and the population is constant, that is, the number of 'natural' COVID-19 unrelated deaths is balanced by p_S , and so $p_S = \mu N$ and p_{Efc}, \dots, p_R vanish and the disease-related deaths that happened on the way to the DFE are not included, that is, $d_I = d_H = 0$, since the DFE excludes any infection. We let the solution

$$\mathbf{x}(t) = (S(t), E_{fc}(t), E_{pc}(t), I_{fc}(t), I_{pc}(t), H(t), R(t)),$$

represent the trajectory of the system in \mathbb{R}_+^7 , for $0 \leq t \leq T$. Then, the DFE contains only susceptibles, that is,

$$DFE = (N, 0, 0, 0, 0, 0, 0),$$

and the force of infection vanishes, $\Gamma = 0$.

Table 1: Parameters of the model and their description.

Parameter	Description
$N(t)$	total population (at time t), (8)
μ	'natural' death rate coefficient, fixed
$\theta(t); (1 - \theta(t))$	fractions of fully and partially compliant exposed
p_S	recruitment rate of susceptibles
$p_{E_{fc}}; p_{E_{pc}}$	recruitment rates of fully and partially compliant exposed
$p_{I_{fc}}; p_{I_{pc}}$	recruitment rates of fully and partially compliant infectives
p_H	recruitment rate of hospitalized
p_R	recruitment rate of recovered
$\epsilon_{E_{fc}}; \epsilon_{E_{pc}}$	factors in the transmission rates by exposed
$\epsilon_{I_{fc}}; \epsilon_{I_{pc}}$	factors in the transmission rates by infectives
ϵ_H	a factor in transmission rate by hospitalized
$\gamma_{fc}; \gamma_{pc}$	rates of developing clinical symptoms in exposed
γ^-	crossing rate from E_{fc} to I_{pc}
γ^+	crossing rate from E_{pc} to I_{fc}
$\gamma_E; \gamma_I$	rates between fully and partially compliant exposed and infectives
δ	rate of hospitalization of infectives
d_I	disease-induced death rates of infectives
d_H	disease-induced death of hospitalized
σ_E	recovery rate of exposed
σ_I	recovery rate of infectives
σ_H	recovery rate of hospitalized
δ_*	infectiveness rate increase factor with infected
δ^*	infectiveness rate decrease factor with recovered
$\beta_*; \beta^*$	lower and upper bounds on the contact rate
β_0	initial contact rate
$E_{fc0}; E_{pc0}$	initial values of exposed populations
$I_{fc0}; I_{pc0}$	initial values of infected populations
$H_0; R_0$	initial values of hospitalized and recovered

We note that the model contains 29 parameters and seven initial conditions. However, in the computations we use three theta values instead of one so there are 31 parameters and seven initial conditions, which are optimized. The Jacobian of the system (see Appendix A) evaluated at the DFE is given by

$$J(DFE) = \quad (27)$$

$$\begin{pmatrix} -\mu & -\beta\epsilon_{E_{fc}} & -\beta\epsilon_{E_{pc}} & -\beta\epsilon_{I_{fc}} & -\beta\epsilon_{I_{pc}} & -\beta\epsilon_H & 0 \\ 0 & \theta\beta\epsilon_{E_{fc}} - \widehat{\gamma}_{fc} & \theta\beta\epsilon_{E_{pc}} & \theta\beta\epsilon_{I_{fc}} & \theta\beta\epsilon_{I_{pc}} & \theta\beta\epsilon_H & 0 \\ 0 & (1-\theta)\beta\epsilon_{E_{fc}} & (1-\theta)\beta\epsilon_{E_{pc}} - \widehat{\gamma}_{pc} & (1-\theta)\beta\epsilon_{I_{fc}} & (1-\theta)\beta\epsilon_{I_{pc}} & (1-\theta)\beta\epsilon_H & 0 \\ 0 & \gamma_{fc} & \gamma^- & -\widehat{\delta} & 0 & 0 & 0 \\ 0 & \gamma^+ & \gamma_{pc} & 0 & -\widehat{\delta} & 0 & 0 \\ 0 & 0 & 0 & \delta & \delta & -\widehat{\sigma}_H & 0 \\ 0 & \sigma_E & \sigma_E & \sigma_I & \sigma_I & \sigma_H & -\mu \end{pmatrix}$$

where $\widehat{\gamma}_{fc}$, $\widehat{\gamma}_{pc}$, and $\widehat{\delta}$ are defined in (18)–(20) and

$$\widehat{\sigma}_H = \sigma_H + d_H + \mu. \quad (28)$$

We remark that a rather technical and involved analysis is needed to establish rigorously that when the DFE is stable and attracting,

$$\lim_{t \rightarrow \infty} \mathbf{x}(t) = DFE,$$

for all nonnegative initial conditions, and the EE does not exist. And when the DFE loses its stability, the EE appears and is stable and attracting. We leave this theoretical question open here and remark about it in Section 8.

6 Numerical Simulations

This section describes the approach to our computer simulations of the model. We use MATLAB's `ode45` ODEs solver together with `fmincon` constrained optimization routine to determine the value of the optimized model parameters that minimize the ℓ^1 -deviation of the model predictions for the total number of cases and deaths and the seven-day averaged numbers of daily cases and deaths from the given data. To be specific, to find some of the model parameters, we minimize the objective function:

$$\begin{aligned} \Psi(\omega) := & \sum_{n=1}^{N_{data}} |CC(\omega, t_n) - \widehat{CC}_n| + \sum_{n=1}^{N_{data}} |CD(\omega, t_n) - \widehat{CD}_n| \\ & + \sum_{n=1}^{N_{data}} |DC(\omega, t_n) - \widehat{DC}_n| + \sum_{n=1}^{N_{data}} |DD(\omega, t_n) - \widehat{DD}_n|, \end{aligned}$$

where N_{data} is the total number of data points, $\omega \in \mathbb{R}^{38}$ is the parameter set, $CC(\omega, t_n)$, $CD(\omega, t_n)$, $DC(\omega, t_n)$ and $DD(\omega, t_n)$ are the model predictions using ω for the cumulative cases, cumulative deaths, daily cases and daily deaths, respectively, on day n , and \widehat{CC}_n , \widehat{CD}_n , \widehat{DC}_n and \widehat{DD}_n denote the actual reported cumulative cases, cumulative deaths, 7-day averages of the daily cases, and daily deaths, respectively, on day n .

Table 1 summarizes the meaning of the model parameters in ω . For the model to make sense, we impose the following constraints:

$$\widehat{\gamma}_{fc} + |\gamma_E| < 1, \quad \widehat{\gamma}_{pc} + |\gamma_E| < 1, \quad \widehat{\delta} + |\gamma_I| < 1, \quad \widehat{\sigma} < 1, \quad (29)$$

where $\widehat{\gamma}_{fc}$, $\widehat{\gamma}_{pc}$, $\widehat{\delta}$, $\widehat{\sigma}$ are defined in (18)–(20), and (5). The first condition in (29) guarantees that in equation (2) the number of those that leave compartment E_{fc} , per day, does not exceed the number of the individuals in that compartment. The other conditions in (29) have similar interpretations.

Table 2: Optimized model parameter values for South Korea

parameter	optimized value	units	interval
$N(0)$	$51 \cdot 10^6$	indiv	fixed
μ	$1.7 \cdot 10^{-5}$	1/day	fixed
$\theta_1; \theta_2; \theta_3$	0.0101, 0.995, 0.352	-	[0.01, 0.25]; [0.1, 0.995]; [0.35, 0.75]
p_S	124	indiv/day	[0, 870]
$p_{E_{fc}}; p_{E_{pc}}$	0; 6.2359	indiv/day	[0, 870]; [0, 100]
$p_{I_{fc}}; p_{I_{pc}}$	0.1037; 0.0732	indiv/day	[0, 10]; [0, 10]
p_H	0.0	indiv/day	[0, 5]
p_R	4.6508	indiv/day	[0, 5]
$\epsilon_{E_{fc}}; \epsilon_{E_{pc}}$	0.05; 0.9	-	[0.05, 0.6]; [0.25, 0.90]
$\epsilon_{I_{fc}}; \epsilon_{I_{pc}}$	0.3; 0.4	-	[0.30, 0.85]; [0.4, 0.75]
ϵ_H	0.005	-	[0.005, 0.2]
$\gamma_{fc}; \gamma_{pc}$	0.085; 0.04	1/day	[0.01, 0.085]; [0.04, 0.15]
$\gamma^-; \gamma^+$	0.001216; 0.085	1/day	[0.0005, 0.0035]; [0.005, 0.085]
$\gamma_E; \gamma_I$	0.04486 -0.04261	1/day	[-0.1, 0.1]; [-0.1, 0.1]
δ	0.008	1/day	[0.001, 0.008]
d_I	0.0005203	1/day	[0.00025, 0.005]
d_H	0.04909	1/day	[0.01, 0.05]
σ_E	0.05067	1/day	[0.01, 0.15]
σ_I	0.15	1/day	[0.01, 0.15]
σ_H	0.01819	1/day	[0.005, 0.1]
$\delta_*; \delta^*$	0.7292; 0.2982	$1/(\text{indiv})(\text{day})^2$	[0.005, 0.75]; [0.05, 0.95]
$\beta_*; \beta^*$	0.05; 0.5	$1/(\text{indiv})(\text{day})^2$	[0.001, 0.5]; [0.001, 0.6]
β_0	0.1133	1/day	[0.001, 0.6]
$E_{fc0}; E_{pc0}$	103.7; 2584	indiv	[0, 500]; [0, 5000]
$I_{fc0}; I_{pc0}$	1.079; 7.29	indiv	[0, 100]; [0, 100]
$H_0; R_0$	4.147; 10	indiv	[0, 10]; [0, 10]

7 COVID-19 in The Republic of Korea

This section presents the model simulations of the pandemic's dynamics in South Korea, which is chosen because it is one of the first countries that went through the pandemic cycle and the complete unbiased data is available on the web, in particular in (Worldometer 2021). As of Aug. 8, 2020, the pandemic there is under control, with minor outbreaks. The values of the optimized baseline parameters and their intervals of feasibility can be found in Table 2. The total population $N(0)$ and the COVID-19 unrelated death rate μ are fixed constants obtained from South Korea's population data and are not part of the optimization process. We solved the ODEs of Model 1 numerically using these optimized parameters predicting the pandemic's near future.

As noted above, the values in Table 2 were obtained by an ℓ^1 optimization routine in MATLAB that compares the model predictions for the total number of cases and the total number of deaths as well as the seven-day averaged daily cases and deaths with the data taken from (Worldometer 2021) for the time period of 100 days, from 15 Feb. until 25 May 2020. It is important to emphasize that the model uses past data and, therefore, cannot predict outcomes resulting from major changes in the virus behavior, new mutations, change in population behavior, new policies and directives, or the environment. However, the model predictions for the following 75 days are very close to what

was observed in the field, as we show below. Then, by modifying only θ , the model predictions can fit very well for more than a year.

7.1 Baseline simulations

We start with the baseline simulation, using the parameters in Table 2. To properly describe the South Korean government's response to the pandemic, we use the following values of θ : the lock-down order was declared on day 8, and the relaxation of the directive started on day 81. To represent these policy changes in the model, we set

$$\theta = \begin{cases} \theta_1 = 0.01 & \text{if } t < 8, \\ \theta_2 = 0.995 & \text{if } 8 \leq t < 81, \\ \theta_3 = 0.352 & \text{if } 81 \leq t \leq 175. \end{cases}$$

These values were obtained by the optimization subroutine and in particular, we note that $\theta = 0.995$ for days 8 – 80 corresponds to very effective control directives and a highly compliant population.

The cumulative number of COVID-19 cases and the cumulative number of deaths are depicted in Figure 2 for the period of 175 days, from 15 Feb. until 8 Aug. 2020. The red filled circles are the field data for the first 100 days of the pandemic (15 Feb. until 25 May), (Worldometer 2021), which were used to optimize the parameters, while the green filled squares depict subsequent data (26 May till 8 Aug.). The agreement between the green filled squares and the blue line, which is a measure of the model's predictive ability, is good for the cumulative number of cases, although it slightly under-predicts the more recent cases, however, the prediction is remarkable for the total deaths. We note the model does not fully capture the initial exponential growth in the number of cases, while it does so well with the number of deaths. The median discrepancy in the cumulative cases is 182 and the median error in the cumulative deaths is 4.4.

Fig. 3 depicts the daily cases and deaths, respectively, for the same simulations. To allow for a better comparison, in addition to the data (red filled circles and green filled squares) we also introduce, similarly to various web publications, a seven-day moving average (red curve), i.e., averaging the data over the previous seven days (or a part of them at the beginning). Even though there is considerable randomness in the daily data while the simulations don't admit randomness, and the numbers of cases are rather small, the daily case predictions follow the trends surprisingly well. We conclude that the model captures well the known details of the pandemic in South Korea.

Furthermore, the form of the model allows us to investigate the behavior of the other subpopulations, which are usually hard to assess and are not reported separately. This provides further details and considerable insight into the disease dynamics. Fig. 4 depicts the model predictions of (for the sake of simplicity) the combined daily numbers of exposed, $E_{fc} + E_{pc}$, and of infected $I_{fc} + I_{pc}$, noting that the corresponding data is not available (in open sources).

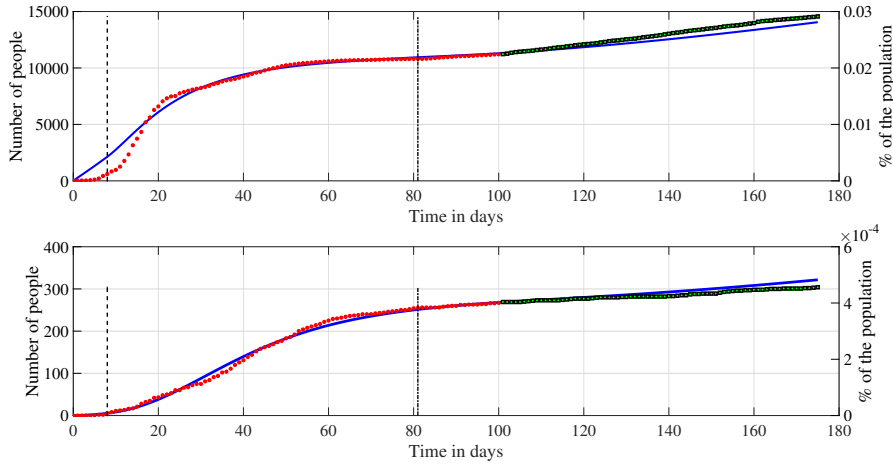


Fig. 2: Model predictions (blue curves) of the cumulative cases (top) and deaths (bottom); 175 days from 15 Feb. until 8 Aug. 2020. The red filled circles are the 100 days of field data used in the optimization, the green filled squares depict subsequent data. θ changed from $\theta_1 = 0.010$ to $\theta_2 = 0.995$ on day 8 (vertical dashed lines) and to $\theta_3 = 0.352$ on day 81 (vertical dash-dotted lines). The median error in the cumulative cases was 182 and the maximum error was 1847 (on day 11); the median error in the cumulative deaths was 4.4 and the maximum error was 18 (on day 174).

Fig. 5 depicts the simulation results for the other three subpopulations: the number of susceptibles S (top left), the number of hospitalized H (top right) and the number of recovered R (bottom left). The number of hospitalized H should be known precisely to the authorities, but it was not available online for comparison. Finally, and this is one of the main contributions of this work, we show in Fig. 5 (lower right) that the decrease in the contact rate β in the South Korea case over 175 days is very small. This is likely due to their success in the first 175 days in controlling the spread of the disease. Running the simulation for 1,000 days shows a decrease to $\beta = 0.094$ hence as time increases β changes more noticeably. For countries with uncontrolled disease spread we expect more significant variation in β . Therefore, considering the infection rate as a dependent variable in that case would lead to more accurate model predictions.

To determine the stability of the DFE, we found numerically the eigenvalues of the Jacobian at the DFE using (27). We used the baseline parameters, except for setting $p_S = \mu N$, $p_{I_{fc}} = \dots = p_R = 0$, $d_I = d_H = 0$, so that the population is constant, $\beta = 0.094$, and $\theta = 0.995$. Then, the eigenvalues were approximately

$$-1.710^{-5}, -1.710^{-5}, -0.273, -0.0188, -0.089, -0.102, -0.158.$$

Thus, (when $\theta = 0.995$) all the eigenvalues are real and negative, so the DFE is stable and attracting.

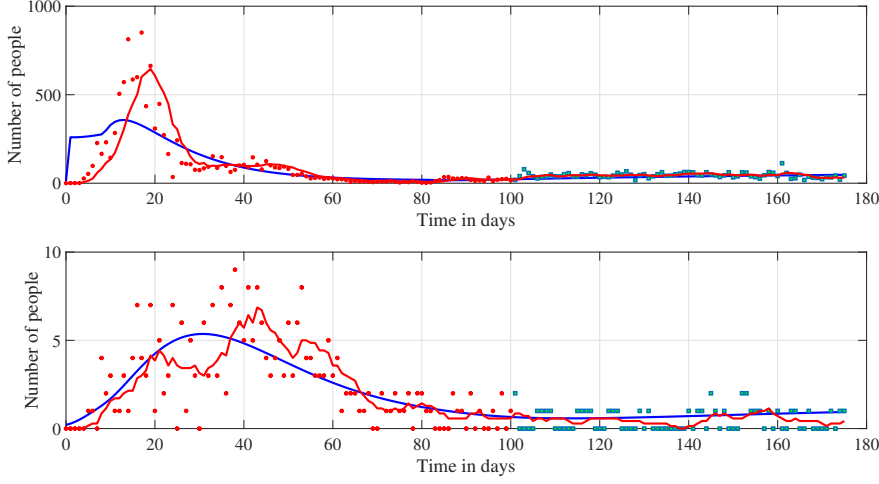


Fig. 3: Model predictions (blue curves) of the daily cases of infection (top) and deaths (bottom), and seven-day moving averages of the data (red curves); 175 days from 15 Feb. until 8 Aug. 2020. The red filled circles are the 100 days of field data used in the optimization, the green filled squares depict subsequent data. The red curves are the seven-day moving averages of the data. θ changed from $\theta_1 = 0.01$ to $\theta_2 = 0.995$ on day 8 and to $\theta_3 = 0.352$ on day 81.

Hypothetical long runs with $\theta = 0.995$ result in very slow convergence to the DFE, because the first two eigenvalues are very close to zero. Indeed, it took over 1,000 days to see partial convergence to the limit.

As noted above, we found that the DFE loses its stability at $\theta^* \approx 0.034$, which is a bifurcation value when the real part of at least one of the eigenvalues becomes positive, and the DFE becomes unstable. Then, theoretically, the EE appears. Long-time simulations with $\theta = 0.352$, the value on day 81 when the directives were relaxed (which is above the critical value), show, as expected, that the DFE is stable and attracting.

Using the baseline parameters, except for $p_S = \mu N$, $p_{I_{fc}} = \dots = p_R = 0$, $d_I = d_H = 0$, $\beta = 0.094$, and $\theta = 0.352$, shows that the eigenvalues of the Jacobian at the DFE are approximately

$$-1.7 \cdot 10^{-5}, \quad -1.7 \cdot 10^{-5}, \quad -0.0242, \quad -0.0184, \quad -0.2384, \quad -0.1517, \quad -0.1580.$$

Thus, (when $\theta = 0.352$) the DFE is stable and after running the simulation for 1,000 days (with constant population of 51 million), we found approximately

$$S = 50,971,000, \quad E_{fc} = 0, \quad E_{pc} = 0, \quad I_{fc} = 0, \quad I_{pc} = 0, \quad H = 0, \quad R = 29,000.$$

Since there are no new infections, $R \rightarrow 0$ because of natural deaths, but very slowly.

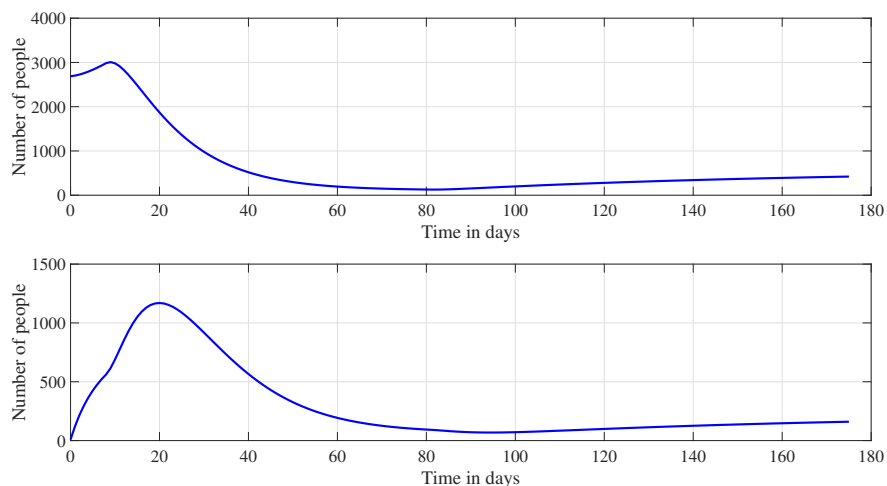


Fig. 4: Baseline simulation. The combined exposed ($E_{fc} + E_{pc}$) (top) and the combined infected ($I_{fc} + I_{pc}$) (bottom). 175 days from 15 Feb. until 8 Aug. 2020. θ changed from $\theta_1 = 0.01$ to $\theta_2 = 0.995$ on day 8 and to $\theta_3 = 0.352$ on day 81.

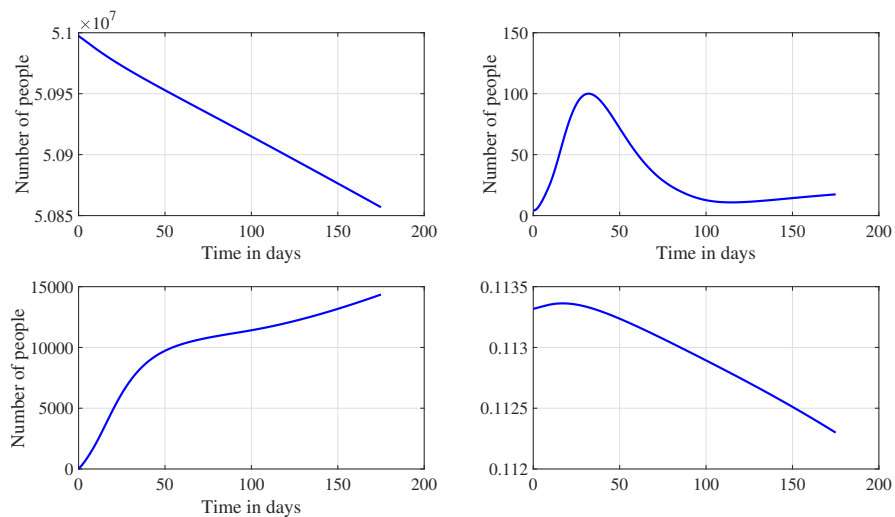


Fig. 5: Baseline simulation. The daily numbers of susceptibles S (top left); hospitalized H (top right); recovered R (bottom left); and the slight decrease in the disease infectivity β (bottom right). 175 days from 15 Feb. until 8 Aug. 2020. θ changed from $\theta_1 = 0.01$ to $\theta_2 = 0.995$ on day 8 and to $\theta_3 = 0.352$ on day 81.

Model simulations with the baseline parameters for 175 days gives for the cumulative cases, deaths, and asymptomatics, respectively (approximately):

$$CC = 14,058, \quad CD = 322, \quad CA = 5,634,$$

and

$$CFR = 0.022, \quad IFR = 0.016.$$

Simulations with baseline parameters listed in Table 2 for 1,000 days (i.e., asymptotically) yields the following projections:

$$CC = 53,216, \quad CD = 1,188, \quad CA = 23,312,$$

$$CFR = 0.021, \quad IFR = 0.015.$$

We see that the CFR and the IFR are essentially constant. We refer to Subsection 7.3 for additional discussion.

We remark that at the end of 1,000 days, β decreased to $\beta = 0.094$, which indicates that allowing β to be a variable may be of importance. On the other hand, since there were changes in the various directives following day 175, our asymptotic numbers on day 1,000 are more of an ‘if’ case.

We next note that in Spain (Pollán et al. 2020), about a third of the individuals who have developed antibodies were asymptomatic, that is, they did not develop any clinical symptoms and were undocumented until tested for antibodies. Using (16), we obtain that the fractions of such cases in South Korea for 175 days and for 1,000 days, respectively, are:

$$\frac{5,634}{14,058} \approx 40.1\%, \quad \frac{23,312}{53,216} \approx 43.8\%.$$

Therefore about 40% of the infections were not detected. This implies that asymptomatic infections contribute silently but substantially to the spread of the disease and more widespread testing for asymptomatics may be necessary.

Since our model predictions for the first 175 days agree well with the data, we have enough confidence in our model to proceed with the study of the other aspects of the pandemic.

7.2 Effectiveness of control and θ

We study next the effectiveness of the control measures in South Korea that are used to contain the pandemic, lumped together, and described in the model by the parameter θ . To that end, we conduct three hypothetical computer experiments showing the model predictions for different control measures. We use three other values of θ , representing different responses of the government and the population to the pandemic. In these simulations, the θ values are applied on day one and do not change over the 175 days of simulation. In the first simulation, we choose $\theta = 0.5$, which means that there are some control measures but they are not very strict; in the second simulation $\theta = 0.2$; and in the third simulation, $\theta = 0.1$, that is, very few control measures are in place. All the other system parameters are kept at their baseline values reported in Table 2. We note in passing that if any one of these cases was realized, some

of the system parameters would have been different, and it is very likely that the outcome would have been worse.

Fig. 6 shows that when $\theta = 0.5$ the number of cumulative cases and deaths on day 175 (8 Aug. 2020) would increase 1.3-fold approximately. Specifically, on that day the predicted cases would be about 19,739 and deaths about 425, whereas the real data was at 14,562 and 304, respectively.

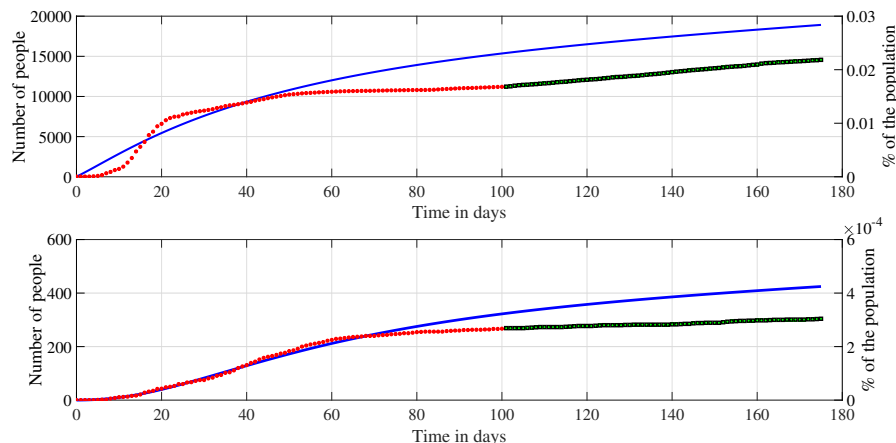


Fig. 6: Simulation with $\theta = 0.5$. Model predictions (blue curves) of the cumulative cases (top) and deaths (bottom); over 175 days from 15 Feb. until 8 Aug. 2020. The red filled circles are the 100 days of field data used in the optimization, the green filled squares depict subsequent data.

Next, Fig. 7 shows that when $\theta = 0.2$, the number of cumulative cases would be more than 5-fold and the number of deaths on day 175 would be more than 4-fold. Specifically, the model predicts that on day 175 there would be about 73,288 cases and 1,276 deaths.

Finally, it is seen in Fig. 8 that if $\theta = 0.1$ the number of cumulative cases on day 175 would have jumped more than 10-fold and the number of cumulative deaths more than 7-fold. Specifically, on day 175, the model predicts about 158,613 cases and 2,387 deaths.

Furthermore, it is common sense to expect that less control measures would lead to worse outcomes and this is confirmed by our model predictions showing substantially worse consequences with relaxed control measures. Indeed, higher values of θ are quite effective in avoiding large scale disruptions of the health care system, and all other state and economic systems because of the pandemic.

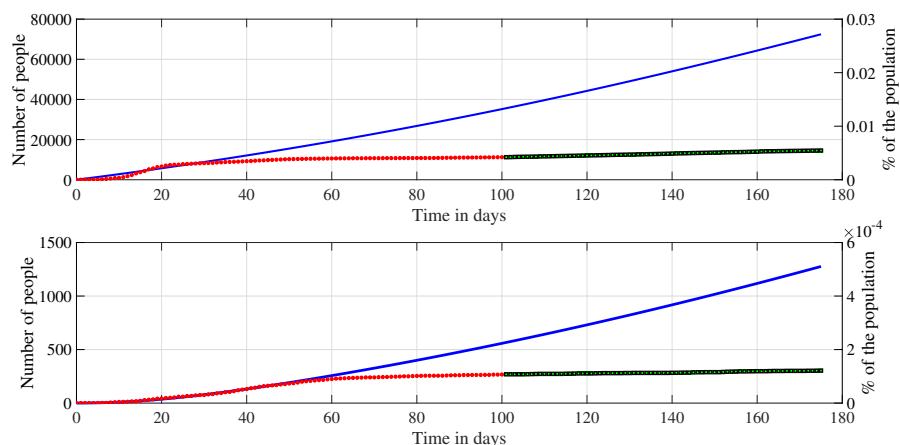


Fig. 7: Simulation with $\theta = 0.2$. Cumulative cases (top) and cumulative deaths (bottom). Model predictions (blue curves) of the cumulative cases (top) and deaths (bottom); over 175 days from 15 Feb. until 8 Aug. 2020. The red filled circles are the 100 days of field data used in the optimization, the green filled squares depict subsequent data.

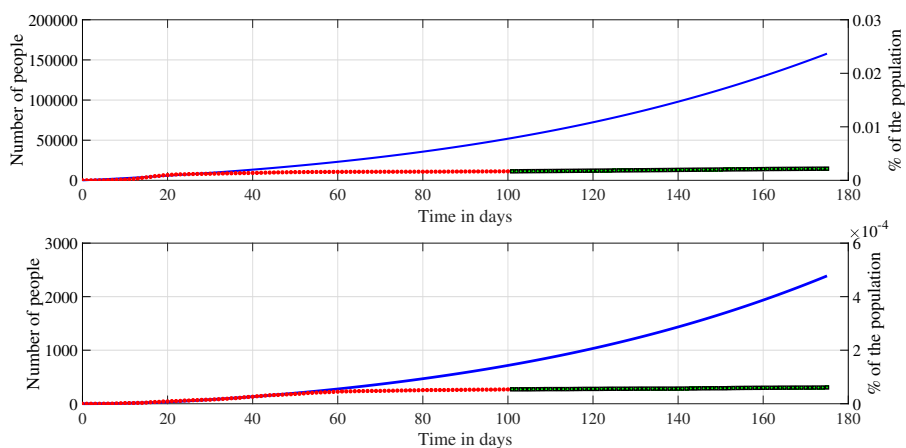


Fig. 8: Simulation with $\theta = 0.1$. Cumulative cases (top) and cumulative deaths (bottom).

7.3 The COVID-19 death rates in South Korea

Since **there is a considerable discussion** in the literature and especially in the media, about the COVID-19 death rates, we use the baseline simulations to determine two death rates, (see, e.g., (Wikipedia 2020a)). The first, the *case fatality rate* (CFR), $\mu_{cov19}^{**}(t)$, is the ratio of the total deaths caused by the disease to all those who have been diagnosed (or documented) with the disease, and this includes the current infectives, hospitalized, and those who recovered

or died, and is given by

$$CFR = \mu_{cov19}^{**}(t) = \frac{CD(t)}{CC(t)}.$$

Here, $CD(t)$ is the cumulative number of deaths, (14), and $CC(t)$, (13), is the cumulative number of infected, up to time t . The second, the *infection fatality rate* (IFR), $\mu_{cov19}^*(t)$, is the ratio of the deaths to all those who had the virus, including the asymptomatics, and is given as

$$IFR = \mu_{cov19}^*(t) = \frac{CD(t)}{CC(t) + CA(t)}.$$

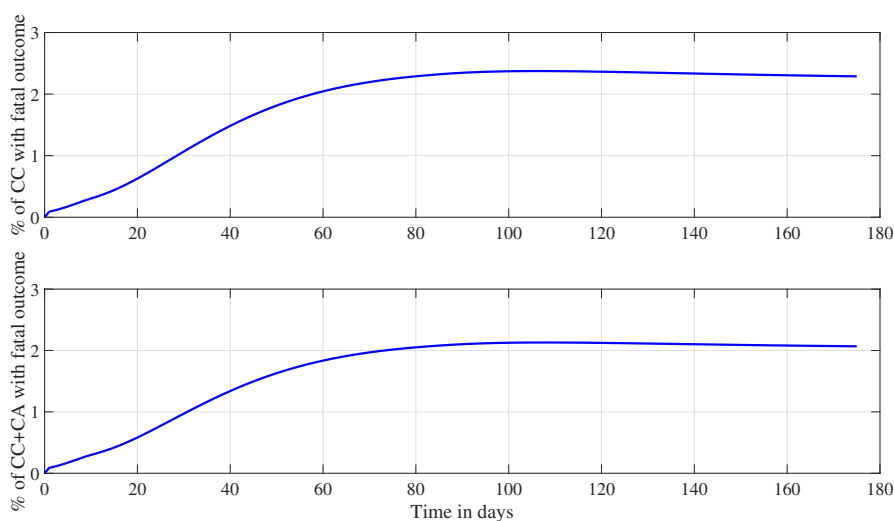


Fig. 9: The death rates (CFR)= μ_{cov19}^{**} , (top) and (IFR)= μ_{cov19}^* (bottom) as functions of time in the baseline simulation.

Fig. 9 shows that on day 175 (8 Aug 2020) the CFR was approximately 2.16% and the IFR was 1.57%. According to the official KCDC (Korea Disease Control and Prevention Agency (KCDC) 2020), on that day there were 304 deaths and 14,562 cases, hence the ‘official’ $CFR = 2.09\%$ was slightly less than the model prediction. Whereas the $CFR = \mu_{cov19}^{**}$ can be found in official publication, the $IFR = \mu_{cov19}^*$ cannot, since it includes those who were never officially counted as having the virus, and usually one has to revert to different ways of estimating it. Thus, our model provides a means to estimate this death rate that has been used (often loosely) in the media.

8 Conclusions and further research

This work presents a new compartmental model of the SEIR-type for the dynamics of the COVID-19 pandemic, in particular allowing the assessment of the effectiveness of the related disease control and containment measures. The model's novelty is two-fold. First, the populations are split into those who follow fully all the control measures and those who follow only partially, such as essential workers who need to be mobile and cannot socially distance, or those who choose to only partially follow the directives. The split is controlled by the parameter θ that also takes indirectly into account the 'quality' of these measures. Second, the infection contact rate coefficient $\beta(t)$ is a dependent variable, the dynamics of which is governed by a differential inclusion, (10). This takes into account the intrinsic variability of β due to various causes of infection rate changes, such as changes in the population behavior or improvements in treatments.

Since the model is complex and includes a differential inclusion, the existence of its unique solution on every finite time interval is established by a nonstandard proof, using results from convex analysis. The positivity of the solutions is also established. Moreover, when the data is measurable with respect to any random variables, then so are the solutions.

Several baseline simulations, in MATLAB, of the disease dynamics were conducted for South Korea. The optimal model parameters were obtained by an (ℓ^1 based) optimization routine fitting the model solutions with the data of both cumulative and daily cases and deaths. In particular, the parameter θ that controls the split between fully and partially compliant populations is found to be 0.010 for the first eight days, on day eight (22 Feb. 2020) when a lock-down and strict control measures were implemented, it jumped to 0.995 and as the control measures started to ease on day 81 (6 May 2020) it dropped to 0.352. The baseline simulations show that the model captures the disease dynamics very well when compared to the data for daily cases and deaths (with seven day moving averages) and cumulative cases and deaths. Furthermore, it provides additional information about the pandemic dynamics that are difficult to observe in the field, such as 40% asymptomatics.

One of the model conclusions, when applied to South Korea, is that their success in controlling and reducing the infection rates is related to having a period of 73 days in which $\theta = 0.995$, which indicates that the majority of the population adhered to the national directives and disease control measures, which in turn were consistent and clearly applied.

In addition, our model predicts substantially worse consequences with relaxed control measures which makes sense as it is common sense to expect that less control measures would lead to worse outcomes. Indeed, higher values of θ are quite effective to avoid large scale disruptions of the health care system, and all other state and economic systems because of the pandemic. This, however, is in the absence of vaccinations.

To gain further insight into the model predictions, we studied the system's equilibrium points. Due to the complexity of the model, instead of finding a

basic stability number \mathcal{R}_C , we used the the eigenvalues of the system Jacobian. We found that the disease-free equilibrium (DFE) is asymptotically stable when $\theta = 0.995$ and becomes unstable when $\theta^* \approx 0.034$, and since we used $\theta = 0.352$ from day 81 onward, the DFE is stable and attracting.

We also used the baseline simulations to compute the death rates and found that the case fatality rate was $CFR = 2.16\%$ and the infection fatality rate was $IFR = 1.57\%$ on day 175, as shown in Fig. 9. The simulations for 1,000 days show that the rates are essentially the same.

The next topic we investigated was the effectiveness of the disease containment measures controlled by the values of θ . Simulations with $\theta = 0.5, 0.2, 0.1$ show that not using sufficient control measures would have caused a substantial increase in the number of cases and deaths. Indeed, for $\theta = 0.1$ there would be more than a 10-fold increase in cases and 7-fold increase in fatalities. These results were obtained without taking into account large-scale vaccination.

An important result that the model provided is that the asymptomatics, those who were carry the virus without symptoms, constituted about 40% of the cases. This is very important information that is very difficult and costly to obtain in the field.

We also performed a partial sensitivity study of the models dependence on θ , and the infection rates of the exposed (γ_{fc}, γ_{pc}). We found that the model is sensitive to these parameters. Thus, to obtain reliable predictions, these model parameters need to be estimated accurately. However, since we did not conduct a full sensitivity analysis with respect to the full set of 38 model parameters, we did not present these impartial results in this work.

We now describe some of the unresolved issues that may be of interest for further study:

- (i) Add the effects of large-scale vaccination to the model and study the model predictions. This will bring the model up-to-date and entails modest modifications of the model.
- (ii) Modify the model to take into account new variants of the SARS-CoV-2. This entails major modifications of the model.
- (iii) Replace the jump of θ to 0.352 after day 81 when the lock-down control measures started to ease, with an appropriate function of time, $\theta = \theta(t)$.
- (iv) Compare the model prediction of the hospitalized $H(t)$, (Fig. 5 top right), and the field data.
- (v) Introduce more θ -like parameters to allow for the separate assessment of the control measures, such as wearing a face mask in public, washing hands often, keeping distance in public spaces, and following the instructions. However, such an expansion may result in a more complex model that may be more difficult to work with.

From the mathematical point of view, it may be of interest to:

Establish rigorously the bifurcation property in θ ; the convergence of the solutions to the DFE when it is stable and attracting, and the convergence to the EE when it exists. Determine that there are no other equilibrium points and analyze in more depth the properties of the two states. Study more thor-

oughly the differential inclusion for β , consider alternative formulations based on more general biological information about the disease based on published observations. Find the optimal regularity of the solutions. Study alternative objective functionals by assigning different weights for the number of cases and deaths and using an ℓ^2 -type minimization.

We conclude that the model has been sufficiently validated for the pandemic in South Korea. It both provides insight and allows for ‘mathematical experiments.’ We plan to use it for other countries and states for which reliable data can be found.

Acknowledgements We would like to thank the referee and the editor for their thorough and helpful comments that improved the work.

Conflicts of interest

The authors did not receive support from any organization for the submitted work. The authors have no conflicts of interest to declare that are relevant to the content of this article.

References

- Al-Asuoad N (2017) *Mathematical Models, Analysis and Simulations in Epidemiology, Population Dynamics, and Heart Tissue*. Ph.D. Dissertation, Oakland University
- Al-Asuoad N, Shillor M (2018) Modeling, analysis and simulations of MERS outbreak in Saudi Arabia. *BIOMATH* 7(1):1802277, <https://doi.org/10.11145/j.biomath.2018.02.277>
- Al-Asuoad N, Rong L, Alaswad S, Shillor M (2016) Mathematical model and simulations of MERS outbreak: Predictions and implications for control measures. *BIOMATH* 5(2):1–21, <https://doi.org/10.11145/j.biomath.2016.12.141>
- Allen LJ (2007) *An Introduction to Mathematical Biology*. Pearson Prentice-Hall
- Anguelov R, Banasiaka J, Bright C, Lubuma J, Ouifki R (2020) The big unknown: The asymptomatic spread of COVID-19. *BIOMATH* pp 1–9, <https://doi.org/10.11145/j.biomath.2020.05.103>
- Báez-Sánchez AD, Bobko N (2020) On equilibria stability in an epidemiological SIR model with recovery-dependent infection rate. *TEMA (São Carlos)* 21:409 – 424, URL http://www.scielo.br/scielo.php?script=sci_arttext&pid=S2179-84512020000300409&nrm=iso
- Boyce W, DiPrima R (1986) *Elementary Differential Equations and Boundary Value Problems*. (4th Edition) Wiley International, John Wiley & Sons, ISBN 0-471-83824-1

- Brézis H (1973) Opérateurs maximaux monotones et semigroupes de contractions dans les espaces de Hilbert, vol 5. North Holland Mathematics Studies Center for Systems Science and Engineering at Johns Hopkins University (JHU) (2021) COVID-19 Coronavirus Pandemic. <https://gisanddata.maps.arcgis.com/apps/opsdashboard/index.html#/bda7594740fd40299423467b48e9ecf6>. Accessed 25 Feb. 2021
- Centers for Disease Control and Prevention (CDC) (2020) COVID-19 Published Science and Research. <https://www.cdc.gov/coronavirus/2019-ncov/more/science-and-research.html>. Accessed 9 July 2020
- Eikenberry SE, Mancuso M, Iboi E, Phan T, Eikenberry K, Kuang Y, Kostelich E, Gumel AB (2020) To mask or not to mask: Modeling the potential for face mask use by the general public to curtail the COVID-19 pandemic. *Infectious Disease Modelling* 5:293–308, <https://doi.org/10.1016/j.idm.2020.04.001>
- Fanelli D, Piazza F (2020) Analysis and forecast of COVID-19 spreading in China, Italy and France. *Chaos Soliton Fract* 134:109761, <https://doi.org/10.1016/j.chaos.2020.109761>
- Gai C, Iron D, Kolokolnikov T (2020) Localized outbreaks in an S-I-R model with diffusion. *J Math Biol* 80:1389–1411, <https://doi.org/10.1007/s00285-020-01466-1>
- Garba SM, Lubuma JMS, Tsanou B (2020) Modeling the transmission dynamics of the COVID-19 pandemic in South Africa. *Mathematical Biosciences* 328:108441, <https://doi.org/10.1016/j.mbs.2020.108441>
- Giordano G, Blanchini F, R Bruno PC, Filippo AD, Matteo AD, Colaneri M (2020) Modelling the COVID-19 epidemic and implementation of population-wide interventions in Italy. *Nat Med* 26:855–860, <https://doi.org/10.1038/s41591-020-0883-7>
- Greenhalgh D, Das R (2020) Modelling epidemics with variable contact rates. *Theor Popul Biol* 47(2):129–79, <https://doi.org/10.1006/tpbi.1995.1006>
- Greenhalgh S, Day T (2017) Time-varying and state-dependent recovery rates in epidemiological models. *Infectious Disease Modelling* 2(4):419–430, <https://doi.org/10.1016/j.idm.2017.09.002>
- Hale JK (2009) *Ordinary Differential Equations*. Dover Publications Inc., URL <https://store.doverpublications.com/0486472116.html>
- Heesterbeek J, Metz JAJ (1993) The saturating contact rate in marriage- and epidemic models. *J Math Biol* 31:529–539, <https://doi.org/10.1007/BF00173891>
- Hethcote HW (2000) The mathematics of infectious diseases. *SIAM Rev* 42(4):599–653, URL <http://www.jstor.org/stable/2653135>
- Hou C, Chen J, Zhou Y, Hua L, Yuan J, He S, Guo Y, Zhang S, Jia Q, Zhao C, Zhang J, Xu G, Jia E (2020) The effectiveness of quarantine of Wuhan city against the Corona Virus Disease 2019 (COVID-19): A well-mixed SEIR model analysis. *J Med Virol* 92(7):841–848, <https://doi.org/10.1002/jmv.25827>

- Huang C, Huang L, Wang Y, Li X, Ren L, Gu X, Kang L, Guo L, Liu M, Zhou X, Luo J, Huang Z, Tu S, Zhao Y, Chen L, Xu D, Li Y, Li C, Peng L, Li Y, Xie W, Cui D, Shang L, Fan G, Xu J, Wang G, Wang Y, Zhong J, Wang C, Wang J, Zhang D, Cao B (2021) 6-month consequences of COVID-19 in patients discharged from hospital: a cohort study. *Lancet* 397(10270):220–232, [https://doi.org/10.1016/S0140-6736\(20\)32656-8](https://doi.org/10.1016/S0140-6736(20)32656-8)
- Johnston MD, Pell B (2020) A dynamical framework for modeling fear of infection and frustration with social distancing in COVID-19 spread. *Math Biosci Eng* 17(6):7892–7915, <https://doi.org/10.3934/mbe.2020401>
- Korea Disease Control and Prevention Agency (KCDC) (2020) The updates on COVID-19 in Korea as of 5 July. <http://www.kdca.go.kr/board/board.es?mid=a30402000000&bid=0030>. Accessed 25 February 2020
- Kuttler KL (2017) *Elementary Differential Equations*. Chapman and Hall/CRC, URL <https://www.routledge.com/Elementary-Differential-Equations/Kuttler/p/book/9781138740914>
- Kuttler KL, Li J, Shillor M (2016) A general product measurability theorem with applications to variational inequalities. *Electron J Differ Eq* 2016(90):1–12, <https://ejde.math.txstate.edu/Volumes/2016/90/kuttler.pdf>
- Marshall M (2010) The lasting misery of coronavirus long-haulers. *Nature* 585(7825):339–341, <https://doi.org/10.1038/d41586-020-02598-6>
- Nextstrain (2020) Genomic epidemiology of novel coronavirus. <https://nextstrain.org/ncov/2020-03-20?m=div>, Accessed 5 June 2020
- O’Neill P (1997) An epidemic model with removal-dependent infection rate. *The Annals of Applied Probability* 7(1):90 – 109, <https://doi.org/10.1214/aoap/1034625253>
- Pollán M, Pérez-Gómez B, Pastor-Barriuso R, Oteo J, Hernán MA, Pérez-Olmeda M, Sanmartín JL, Fernández-García A, Cruz I, de Larrea NF, Molina M, Rodríguez-Cabrera F, Martín M, Merino-Amador P, Paniagua JL, noz Montalvo JFM, Blanco F, Yotti R (2020) Prevalence of SARS-CoV-2 in Spain (ENE-COVID): a nationwide, population-based seroepidemiological study. *Lancet* [https://doi.org/10.1016/S0140-6736\(20\)31483-5](https://doi.org/10.1016/S0140-6736(20)31483-5)
- Richard Bellman KLC (1995) *Modern Elementary Differential Equations*, 2nd Ed. Dover Publications Inc.
- Thieme H (2003) *Mathematics in Population Biology*. Princeton University Press, Princeton
- Thieme HR, Yang J (2002) An endemic model with variable re-infection rate and applications to influenza. *Mathematical Biosciences* 180(1):207–235, [https://doi.org/10.1016/S0025-5564\(02\)00102-5](https://doi.org/10.1016/S0025-5564(02)00102-5)
- Wikipedia (2020a) Case fatality rate. https://en.wikipedia.org/wiki/Case_fatality_rate#Terminology, Accessed 5 July 2020
- Wikipedia (2020b) COVID-19 pandemic. https://en.wikipedia.org/wiki/COVID-19_pandemic. Accessed 5 April 2020
- Wikipedia (2021) Compartmental models in epidemiology. https://en.wikipedia.org/wiki/Compartmental_models_in_epidemiology#Variable_contact_rates. Accessed 3 March 2021

-
- World Health Organization (WHO) (2021) MERS-CoV. https://www.who.int/csr/don/archive/disease/coronavirus_infections/en, Accessed 25 Feb. 2021
- Worldometer (2021) COVID-19 Coronavirus Pandemic. <https://www.worldometers.info/coronavirus>. Accessed 25 Feb. 2021
- Zhang J, Ma Z (2003) Global dynamics of an SEIR epidemic model with saturating contact rate. *Math Biosci* 185(1):15 – 32, [https://doi.org/10.1016/S0025-5564\(03\)00087-7](https://doi.org/10.1016/S0025-5564(03)00087-7)

Appendix A Jacobian of the system

This appendix constructs an expression for the system's Jacobian assuming that $\beta = \text{const}$.

For this purpose, we write equations (1)–(7) using the notation introduced in (5) as

$$\frac{d\mathbf{x}(t)}{dt} = \mathbf{f}(t),$$

where the components of $\mathbf{f}(t)$ are given by

$$\begin{aligned} f_1(t) &= p_S - \Gamma S - \mu S, \\ f_2(t) &= p_{E_{fc}} + \theta \Gamma S - \widehat{\gamma}_{fc} E_{fc} + \frac{\gamma_E}{N} E_{fc} E_{pc}, \\ f_3(t) &= p_{E_{pc}} + (1 - \theta) \Gamma S - \widehat{\gamma}_{pc} E_{pc} - \frac{\gamma_E}{N} E_{fc} E_{pc}, \\ f_4(t) &= p_{I_{fc}} + \gamma_{fc} E_{fc} + \gamma^- E_{pc} - \widehat{\delta} I_{fc} + \frac{\gamma_I}{N} I_{fc} I_{pc}, \\ f_5(t) &= p_{I_{pc}} + \gamma_{pc} E_{pc} + \gamma^+ E_{fc} - \widehat{\delta} I_{pc} - \frac{\gamma_I}{N} I_{fc} I_{pc}, \\ f_6(t) &= p_H + \delta(I_{fc} + I_{pc}) - \widehat{\sigma}_H H, \\ f_7(t) &= p_R + \sigma_E(E_{fc} + E_{pc}) + \sigma_I(I_{fc} + I_{pc}) + \sigma_H H - \mu R. \end{aligned}$$

The Jacobian matrix of the system is

$$J(\mathbf{x}) = \begin{pmatrix} J_{11} & \dots & J_{17} \\ \vdots & \ddots & \vdots \\ J_{71} & \dots & J_{77} \end{pmatrix},$$

where $J_{ij} = \partial f_i / \partial x_j$, $1 \leq i, j \leq 7$. To compute $J(\mathbf{x})$, we note that

$$\begin{aligned} \frac{d\Gamma}{dS} &= -\frac{1}{N}\Gamma, & \frac{d\Gamma}{dE_{pc}} &= -\frac{1}{N}(\Gamma - \beta\epsilon_{E_{pc}}), \\ \frac{d\Gamma}{dE_{fc}} &= -\frac{1}{N}(\Gamma - \beta\epsilon_{E_{fc}}), & \frac{d\Gamma}{dI_{pc}} &= -\frac{1}{N}(\Gamma - \beta\epsilon_{I_{pc}}), \\ \frac{d\Gamma}{dI_{fc}} &= -\frac{1}{N}(\Gamma - \beta\epsilon_{I_{fc}}), & \frac{d\Gamma}{dR} &= -\frac{1}{N}\Gamma, \\ \frac{d\Gamma}{dH} &= -\frac{1}{N}(\Gamma - \beta\epsilon_H), & & \end{aligned}$$

Then, straightforward and rather tedious manipulations yield,

$$\begin{aligned}
J_{11} &= -\Gamma \left(1 - \frac{S}{N}\right) - \mu, \quad J_{12} = \frac{S}{N}(\Gamma - \beta\epsilon_{Efc}), \quad J_{13} = \frac{S}{N}(\Gamma - \beta\epsilon_{Epc}), \\
J_{14} &= \frac{S}{N}(\Gamma - \beta\epsilon_{Ifc}), \quad J_{15} = \frac{S}{N}(\Gamma - \beta\epsilon_{Ipc}), \quad J_{16} = \frac{S}{N}(\Gamma - \beta\epsilon_H), \quad J_{17} = \frac{S}{N}\Gamma, \\
J_{21} &= \theta\Gamma \left(1 - \frac{S}{N}\right), \quad J_{22} = -\theta\frac{S}{N}(\Gamma - \beta\epsilon_{Efc}) - \hat{\gamma}_{fc} + \gamma_E\frac{E_{pc}}{N}, \\
J_{23} &= -\theta\frac{S}{N}(\Gamma - \beta\epsilon_{Epc}) + \gamma_E\frac{E_{fc}}{N}, \quad J_{24} = -\theta\frac{S}{N}(\Gamma - \beta\epsilon_{Ifc}), \\
J_{25} &= -\theta\frac{S}{N}(\Gamma - \beta\epsilon_{Ipc}), \quad J_{26} = -\theta\frac{S}{N}(\Gamma - \beta\epsilon_H), \quad J_{27} = -\theta\frac{S}{N}\Gamma - \frac{\gamma_E}{N^2}E_{fc}E_{pc}, \\
J_{31} &= (1 - \theta)\Gamma \left(1 - \frac{S}{N}\right), \quad J_{32} = -(1 - \theta)\frac{S}{N}(\Gamma - \beta\epsilon_{Efc}) - \gamma_E\frac{E_{pc}}{N}, \\
J_{33} &= -(1 - \theta)\frac{S}{N}(\Gamma - \beta\epsilon_{Epc}) - \hat{\gamma}_{pc} - \gamma_E\frac{E_{fc}}{N}, \quad J_{34} = -(1 - \theta)\frac{S}{N}(\Gamma - \beta\epsilon_{Ifc}), \\
J_{35} &= -(1 - \theta)\frac{S}{N}(\Gamma - \beta\epsilon_{Ipc}), \quad J_{36} = -(1 - \theta)\frac{S}{N}(\Gamma - \beta\epsilon_H), \\
J_{37} &= -(1 - \theta)\frac{S}{N}\Gamma + \frac{\gamma_E}{N^2}E_{fc}E_{pc}, \\
J_{41} &= -\gamma_I\frac{I_{fc}I_{pc}}{N^2}, \quad J_{42} = \gamma_{fc} - \gamma_I\frac{I_{fc}I_{pc}}{N^2}, \quad J_{43} = \gamma^- - \gamma_I\frac{I_{fc}I_{pc}}{N^2}, \\
J_{44} &= -\hat{\delta} + \gamma_I\frac{I_{pc}}{N} - \gamma_I\frac{I_{fc}I_{pc}}{N^2}, \quad J_{45} = \gamma_I\frac{I_{fc}}{N} - \gamma_I\frac{I_{fc}I_{pc}}{N^2}, \\
J_{46} &= -\gamma_I\frac{I_{fc}I_{pc}}{N^2}, \quad J_{47} = -\gamma_I\frac{I_{fc}I_{pc}}{N^2} \\
J_{51} &= \gamma_I\frac{I_{fc}I_{pc}}{N^2}, \quad J_{52} = \gamma^+ + \gamma_I\frac{I_{fc}I_{pc}}{N^2}, \quad J_{53} = \gamma_{pc} + \gamma_I\frac{I_{fc}I_{pc}}{N^2}, \\
J_{54} &= -\gamma_I\frac{I_{pc}}{N} + \gamma_I\frac{I_{fc}I_{pc}}{N^2}, \quad J_{55} = -\hat{\delta} - \gamma_I\frac{I_{fc}}{N} - \gamma_I\frac{I_{fc}I_{pc}}{N^2}, \\
J_{56} &= \gamma_I\frac{I_{fc}I_{pc}}{N^2}, \quad J_{57} = \gamma_I\frac{I_{fc}I_{pc}}{N^2}, \\
J_{61} &= 0, \quad J_{62} = 0, \quad J_{63} = 0, \quad J_{64} = \delta, \quad J_{65} = \delta, \quad J_{66} = -\hat{\sigma}_H, \quad J_{67} = 0, \\
J_{71} &= 0, \quad J_{72} = \sigma_E, \quad J_{73} = \sigma_E, \quad J_{74} = \sigma_I, \quad J_{75} = \sigma_I, \quad J_{76} = \sigma_H, \quad J_{77} = -\mu.
\end{aligned}$$